CNWRA *A center of excellence in earth sciences and engineering*

A Division of Southwest Research Institute™
6220 Culebra Road • San Antonio, Texas, U.S.A. 78228-5166
(210) 522-5160 • Fax (210) 522-5155

June 28, 2002
Contract No. NRC–02–97–009
Account No. 20.01402.471

U.S. Nuclear Regulatory Commission
ATTN: Dr. Philip S. Justus
Office of Nuclear Material Safety and Safeguards
TWFN Mail Stop 7 C6
Washington, DC 20555

Subject: Orthogonal jointing during coeval igneous degassing and normal faulting, Yucca Mountain, Nevada—Journal Article (IM 01402.471.130)

Dear Dr. Justus:

The purpose of this letter is to transmit the revised milestone, Orthogonal jointing during coeval igneous degassing and normal faulting, Yucca Mountain, Nevada—Journal Article (IM 01402.471.130). This milestone was originally submitted to NRC on August 17, 2001. Acceptance of the milestone was documented in a letter from Justus to McKague dated October 2, 2001, along with comments and suggestions for improving the milestone. The attached journal manuscript has been revised according to the suggestions and clarifying questions from NRC, which significantly contributed to improving the manuscript. The basic conclusions, however, remain the same. The manuscript discusses the origin of two orthogonal sets of joint swarms mapped on pavements of the Tiva Canyon tuff in the northern part of Yucca Mountain. These joints are characterized by subhorizontal degassing features (tubular structures). Conclusions presented in the manuscript include the joint sets formed very soon after tuff emplacement and were present during degassing and formation of lithophysae in the tuff. Joint formation was influenced by a perturbed stress field, perhaps caused by movement on local normal faults.

The fracture framework of Yucca Mountain provides the primary porosity and permeability through which groundwater moves and is an important consideration with respect to rockfall and determination of optimal drift orientation for the proposed high-level radioactive waste repository. This manuscript is a substantial contribution to understanding the fracture framework of Yucca Mountain.

If you have any questions please contact Dr. David Ferrill at 210-522-6082 or me at 210-522-5183.

Sincerely,
H. Lawrence McKague
GLGP Element Manager

rae
Attachment
cc: J. Linehan, W. Reamer, B. Leslie, D. DeMarco, E. Whitt, B. Meehan, L. Campbell, J. Greeves, J. Schlueter, S. Wastler, T. Essig, K. Stablein, W. Patrick, CNWRA Dirs (ltr only), CNWRA EMs (ltr only), D. Ferrill, B. Hill, P. La Femina, D. Waiting, R. Fedors, T. Nagy (SwRI Contracts), W. Dunne, J. Crider, A. Morris

D:\GLGP Group\letters\sds\paper06-28-2002hlm.wpd

Washington Office • Twinbrook Metro Plaza #210
12300 Twinbrook Parkway • Rockville, Maryland 20852-1606

Orthogonal jointing during coeval igneous degassing and normal faulting, Yucca Mountain, Nevada

William M. Dunne[1], David A. Ferrill[2], Juliet G. Crider[3], Brittain E. Hill[2],

Peter C. La Femina[2], Deborah J. Waiting[2], Alan P. Morris[4], Randall W. Fedors[2]

[1]*Department of Geological Sciences,*

University of Tennessee, Knoxville, TN, 37996, USA

[2]*Center for Nuclear Waste Regulatory Analyses,*

Southwest Research Institute, San Antonio, TX, 78238, USA

[3]*Department of Geology, Western Washington University, Bellingham, WA, 98225, USA*

[4]*Department of Earth and Environmental Sciences,*

The University of Texas at San Antonio, San Antonio, TX, 78249, USA

ABSTRACT

An orthogonal system of tube-bearing fractures contains the oldest fractures in the Tiva Canyon Tuff at Yucca Mountain, Nevada. The fractures formed within a month of tuff deposition prior to major degassing. The system consists of narrow persistent NE-trending swarms of fractures with trace lengths typically greater than 5 m and fracture spacings of less than 20 cm, and NW-trending swarms that have a more en echelon geometry and greater fracture spacing than the NE-trending swarms. Spacing for both swarm trends is about 50 meters. Questions concerning the fractures include: (1) determining driving stress(es) for their formation, particularly as they are not consistent with regional stress geometry at the time of their formation; (2) determining the mechanism by which horizontal principal stresses were

reoriented so as to yield orthogonal geometry; and (3) developing insights for predicting fracture geometry in unexposed rock volumes by understanding fracture origin. These questions are important because the fractures may affect the performance of a proposed high-level nuclear waste repository within Yucca Mountain.

We use field data about fracture geometry, field relations of fractures to degassing structures, numerical modeling of fault behavior, and work by previous authors to address these questions. Our interpretation begins with initial eruption and tuff deposition with subsequent or concurrent catastrophic caldera collapse (Christiansen et al., 1977). The ash-flow sheets were deposited over a preexisting topography possibly including a shallow NW-trending basin in the Yucca Mountain area. During initial cooling, fracture swarms formed as elements of orthogonal fumarolic ridge systems where degassing was associated with vertical dilation. Both fracture sets have unusual tubes that are interpreted to have formed during dilation and segmentation of fracture faces resulting from lithophysae formation in the tuff. Modeling of a combination of regional stresses and stress related to slip on local normal faults indicates that they controlled the orientation of the fracture swarms and favored NE-trending fractures forming first. The faults might also have moved in a stress field already perturbed by caldera collapse. Formation of the second NW-trending fractures occurred after a local 90° swap of horizontal principal stress directions due to the presence of the NE-trending swarms, and was possibly aided by differential compaction across the NW-trending basin. Tube-bearing fractures also occur in similar lithostratigraphic units of the Topopah Spring Tuff, which is the stratigraphic interval for the proposed repository for nuclear waste within Yucca Mountain. We believe that they share similar geometric characteristics and formed in a similar manner.

Keywords: orthogonal joints, welded tuffs, cooling joints, degassing tubes, perturbed stress fields, normal faults

INTRODUCTION

We consider the origin of a nearly orthogonal joint system in the Tiva Canyon Tuff and extrapolate the study to other tube-bearing joints at Yucca Mountain, Nevada. The joint system is intriguing because: (1) the two sets comprising the system are orthogonal, (2) both joint sets are clearly associated with tuff degassing, and (3) neither set is perpendicular to the E-W direction of regional extension at the time of formation (Zoback et al., 1981; Morris et al., 1996). Thus, the fractures formed as a system of joints during tuff cooling in response to additional stress components that not only perturbed the regional stress field, but also triggered a 90° rotation of horizontal stress directions, so as to produce both sets of the orthogonal system.

The joint system is also of interest because it is located above the proposed site for the United States of America's first high-level radioactive-waste repository in Yucca Mountain, Nevada. The system is a prominent component of the pathways for shallow ground water infiltration through the capping, moderately to densely welded tuff deposit into the repository (Winograd, 1971; Flint and Flint, 1995; Buesch et al., 1996; Flint et al., 1996). Joints with morphologies similar to those exposed at the surface of Yucca Mountain are also found within the mountain as documented by data collected from the Exploratory Studies Facility (ESF) and Enhanced Characterization of the Repository Block (ECRB) tunnels (Mongano et al., 1999; CRWMS M&O, 2000). Joints that form early in tuffs tend to be relatively large, and represent potential weaknesses that could influence the stability of proposed excavations such as underground waste emplacement drifts. A better understanding of the geometry and origin of

these joints provides a basis for better estimating their importance to the design of underground openings.

In this paper we will: (1) provide a summary of the formation history based on new analyses and published information for the degassing-related joints in a part of the Tiva Canyon Tuff; (2) identify the sources of the driving stresses that may have perturbed the regional stress field to form this orthogonal joint system; and (3) consider causes for the 90° rotation of horizontal stress directions that caused the orthogonal geometry. Although the analysis is conducted in volcanic rocks, the results are applicable to faulted sedimentary rocks with elevated fluid pressures. We use existing field data (e.g., Morgan, 1984; Barton et al., 1984, 1993; Barton and Larsen, 1985; Sweetkind et al., 1995a, 1995b; Throckmorton and Verbeek, 1995), newly gathered field fracture data employing a GPS/GIS approach, new observations of field relationships between joints and volcanogenic features, and numerical modeling of stress field perturbation during active faulting to analyze the origin of this joint system.

DEVELOPING ORTHOGONAL JOINT SYSTEMS

Orthogonal systems of two vertical joints sets are common (Ver Steeg, 1942; Eyal and Reches, 1983; Hancock 1985; Stauffer and Gendzwill, 1987; Dunne and North, 1990; Rawnsley et al., 1992; Martel, 1994; Caputo, 1995; Olson, 1996; Fabbri et al., 2001). Our understanding of their origin is problematic because the orthogonal geometry of the two sets requires at least one 90° change in local principal stress directions during system formation, so that each joint set forms normal to the minimum principal compressive stress. Specifically, the minimum horizontal stress direction (S_h) changes by 90° or swaps with the direction of maximum horizontal stress (S_H). Three groups of mechanism are proposed (Lachenbruch, 1962; Stauffer

and Gendzwill, 1987; Dunne and North, 1990; Caputo, 1995; Olson, 1996): (1) reorienting due to small stress fluctuations between two near-equal horizontal principal stresses ($S_h \sim S_H$), (2) local stress swapping at the scale of individual joints, and (3) regional stress rotation by 90°. Swapping two nearly equal horizontal principal stresses is an intuitively simple scenario, but two nearly equal principal stresses can produce oriented orthogonal systems, random orthogonal systems, or non-orthogonal systems such as columnar cooling joints (Lachenbruch, 1962; Pollard and Aydin, 1988). Thus, this stress state is unlikely to yield the orthogonal geometry. For local swapping, while initial analysis indicated only limited potential (Martel, 1994), recent numerical modeling has shown that local stress swapping is plausible and could occur as a consequence of close spacing in layer-bounded joints (Bai et al., 2002). Regional swapping may occur as a result of regional tectonic changes in stress state over time or relaxation of stresses as a result of uplift and erosion (Engelder, 1985; Hancock, 1985; Stauffer and Gendzwill, 1987; Dunne and North, 1990; Rives et al., 1994; Caputo, 1995). These rotations do not have to occur in a short timeframe, which means that two joint sets with an orthogonal geometry may each form at different times in response to unrelated stress regimes (Gross, 1993; Rawnsley et al., 1998). Thus, both regional and local-scale switching mechanisms may each account for the formation of some orthogonal joint systems.

At Yucca Mountain, identifying the most likely mechanism and scale for triggering the swap that formed the orthogonal joint network is needed. A variety of volcanogenic and tectonic driving stresses is feasible, given that the region was actively extending, that a catastrophic volcanic eruption had just occurred, that the host tuff was still cooling, probably with different temperature gradients through the deposit, that the tuff may have compacted differentially during joint formation, and that normal faults near Yucca Mountain could have moved at that time.

Considering their relative roles during joint formation is necessary to understanding the swapping mechanism.

REGIONAL GEOLOGY

Tectonic Setting

The orthogonal joint system of interest is located in the welded tuffs of the Miocene Tiva Canyon Tuff that was emplaced across the location of the present Yucca Mountain in southwestern Nevada at 12.7 Ma (Fig. 1). Yucca Mountain consists of a thick accumulation of gently east-dipping Miocene volcanic tuff layers cut by an array of major N-trending, W-dipping normal faults, such as the Solitario Canyon, Bow Ridge, and Paintbrush Canyon faults, and NW-trending dextral strike-slip faults (Scott and Bonk 1984; Day et al. 1998a, 1998b; Ferrill et al., 1996, 1999a; Ferrill and Morris, 2001). These faults coevally accommodated active crustal extension within the central Basin and Range Province through the Cenozoic to the present day (Scott, 1990; Wernicke, 1992; Axen et al., 1993; Morris et al., 1996, Day et al., 1998a).

While this period of tectonic activity includes the time of Tiva Canyon volcanism, data supporting fault displacements coeval with volcanism and cooling are limited. The Solitario Canyon fault has several splay faults that exhibit decreasing displacement upward to fault tips in the Tiva Canyon Tuff (Day et al., 1998a), which are interpreted to result from normal faulting before or during deposition of the Tiva Canyon Tuff (Day et al. 1998a). Fridrich (1999) stated that some of the major N-trending faults in the Yucca Mountain region were active between 13.1 and 12.7 Ma from unpublished subsurface thickness data, which includes the eruption time for the Tiva Canyon Tuff. Finally, significant normal fault displacements occurred during the million years after deposition of the Tiva Canyon Tuff based on abrupt changes in thickness of

the overlying 11.6 Ma Rainer Mesa Tuff across faults (e.g., Christiansen et al., 1977; Sawyer et al., 1994; Monsen et al. 1992; Day, et al., 1998a, Fridrich, 1999).

Volcanic Setting

The Tiva Canyon Tuff of the Paintbrush Group is a sequence of pyroclastic flow and minor ash fall deposits that most likely erupted from the Claim Canyon caldera, which is partially preserved on the southern edge of the younger Timber Mountain caldera complex (Fig. 1, 2) (Byers et al., 1976; Buesch et al., 1996). The Tiva Canyon Tuff consists mostly of moderately to densely welded tuffs with devitrification, welding and vapor-phase alteration features that resulted from the eruption of at least 1000 km^3 of compositionally zoned rhyolitic magma at 12.7±0.03 Ma (Byers et al., 1976a; Sawyer et al., 1994). The approximately 100m-thick Tiva Canyon Tuff has two lithostratigraphic members: a thin, crystal-rich upper and a thick, crystal-poor lower member (Buesch et al., 1996). These members formed a single cooling unit (Rosenbaum, 1986). Our study was conducted within the 20-m-thick upper lithophysal zone of the lower crystal-poor member (Buesch et al., 1996).

Variations in underlying topography and depositional thickness affect the cooling behavior of tuff deposits, and potentially their fracture development. The base of the Tiva Canyon Tuff is poorly exposed, so pre-emplacement topography is difficult to identify. Also, the top of the Tiva Canyon Tuff is eroded, obscuring its thickness variations. Still, Fridrich (1999) used surface outcrops and subsurface data to contour the thickness of underlying tuffs from the Paintbrush Group, which may indicate the location of depocenters for the younger Tiva Canyon. Assuming that tuff tops were flat after deposition, he interpreted the data to identify a NW-trending basin directly north of the study area where the underlying Topopah Spring Tuff

thickens 50 m into the depocenter. Also, the small-volume Yucca Mountain and Pah Canyon Tuffs, which are immediately underneath the Tiva Canyon Tuff show the NW-trending paleobasin, and a gentle topographic high that limited tuff deposition immediately to the south (e.g., Day et al., 1998b, Fridrich, 1999).

Tuff Cooling Processes

Tuffs analogous to the Tiva Canyon Tuff are commonly emplaced at temperatures within 100° C of magmatic temperatures, because little cooling occurs during flow except near the basal and upper contacts of the unit (Banks and Hoblitt, 1981; Bursik and Woods, 1996). The Tiva Canyon Tuff likely had a pre-eruption temperature around 700° C (Lipman and Friedman, 1975). Uniform paleomagnetic directions indicate emplacement temperatures above a Curie temperature between 580 and 640° C, and that any rheomorphic deformation occurred above the Curie temperature (Rosenbaum, 1986, 1993).

Degassing occurs rapidly during and subsequent to tuff emplacement at a rate largely controlled by variations in permeability (Miller, 1990; Riehle et al., 1995). Gas pressures initially exceed lithostatic in the upper third of a tuff (Riehle et al., 1995). Trapped gas can form lithophysal cavities through matrix expansion and/or other gas-escape structures along pathways to the surface. Gas pressures within a tuff deposit likely fall below lithostatic within one month after emplacement (Riehle et al., 1995). Gases continue to evolve from the devitrification of volcanic glass through crystallization of anhydrous minerals (e.g., Smith, 1960), triggering vapor-phase crystallization for matrix porosity greater than 20 percent (Sheridan, 1970; Ragan and Sheridan, 1972). Subsequent devitrification and vapor-phase alteration continues to

temperatures as low as 240° C, which probably occurred several years after emplacement for the upper third of the Tiva Canyon Tuff (Lofgren, 1971; Riehle et al., 1995).

The timing of joint development can be evaluated using features related to post-depositional cooling of the tuff deposit. Earliest formed joints would be associated with gas escape structures such as fumaroles, which occur with noticeable alteration mineralization (e.g., Sheridan, 1970; Hildreth, 1983; Keith, 1991, Buesch et al., 1999). Inflationary structures such as lithophysae also form in the earliest stage of degassing. Prelithophysal joints would seldom cut or terminate in lithophysae, may be bent by rheomorphic deformation during lithophysae formation, and will show the effects of vapor-phase mineralization in fracture walls. Compaction and welding continue for time periods on the order of one-to-ten years (Friedman et al., 1963; Riehle, 1973; Bierwirth, 1982, cited in Cas and Wright, 1987; Riehle et al., 1995). Devitrification and vapor-phase mineralization likely continue after compaction ceases, but probably also ceases about a century after emplacement (e.g., Keith, 1991; Riehle et al., 1995). Thus, joints that are post-lithophysae but syn-mineralization will cut or terminate in lithophysae, and show effects of devitrification and vapor-phase mineralization in fracture walls. Finally, joints may form through cooling-induced contraction of the tuff to ambient temperatures (e.g., DeGraff and Aydin, 1987), which can occur more than a century after deposition without associated mineralization or alteration.

JOINT GEOMETRY AND ORIGIN

Previous Work

Since being identified as a potential site for the permanent disposal of high-level nuclear waste, Yucca Mountain has been a focus of several fracture analyses. Fractures have been

investigated at the surface (e.g., Morgan, 1984; Barton et al., 1984, 1993; Barton and Larsen, 1985; Sweetkind et al., 1995a, 1995b; Throckmorton and Verbeek, 1995), in new tunnels (e.g., Albin et al., 1997; Eatman et al., 1997; Mongano et al., 1999), and in boreholes (e.g., Carr, 1992). The early surface analyses used the then novel approach of clearing pavements of about 200 to 250 m^2 (Fig. 3) to investigate fractures as two-dimensional networks (e.g., Barton et al., 1993) rather than relying on scanline or anecdotal station data (Hancock, 1985; La Pointe and Hudson, 1985). The tunnel work combined a rigorously collected line survey (scanline) that sampled 15 fracture attributes with a periphery map of the tunnel walls. It is the largest and most thorough data set about fractures at Yucca Mountain (CRWMS M&O, 2000 and references therein). The tunnel samples almost the entire Paintbrush Group, whereas surface data are mostly from the Tiva Canyon Tuff, which dominates the outcrop on the crest and east flank of Yucca Mountain.

The consensus of the surface investigations, which was also applied to the subsurface work, is that the natural joints at Yucca Mountain have three origins with distinct relative ages based on abutting relationships (Hancock, 1985; Sweetkind and Williams-Stroud, 1996). Volcanic cooling joints are the oldest, largest, most planar natural joints; they commonly have tube structures along their walls (Barton et al., 1984; Sweetkind and Williams-Stroud, 1996; Buesch et al., 1999) (Figs. 4a,b,c, 5). Next, tectonic joints abut against cooling joints, are planar to curviplanar, are larger when fewer older cooling joints are present, and are smooth to rough. Unloading joints are youngest, have hackly irregular surfaces, and are typically subparallel to the ground surface.

A subset of the "cooling" joints as defined by previous workers are the focus of this study. We use the descriptive term "tube-bearing" to refer to these fractures, because the origin

of these joints is questioned here. To the best of our knowledge after an extensive literature search, tube-bearing joints are only found in tuffs at Yucca Mountain. If, as discussed below, these joints formed prior to lithophysae, then the worldwide rarity of tube-bearing joints in welded lithophysal tuffs may reflect the difficulty of similar tuffs to form brittle fractures in the first few days of their existence before lithophysae formation.

Across much of Yucca Mountain, tube-bearing joints occur in two subvertical orthogonal sets that are normal to flow foliation with a locally developed third set that is subhorizontal and parallel to flow layering. This third set is rare, tends to have curviplanar rather than planar geometry, and could simply result from vertical dilation during cooling and degassing, so it is not the focus of our study (Throckmorton and Verbeek, 1995; Sweetkind and Williams-Stroud, 1996). In the central block of Yucca Mountain, the orthogonal sets are typically NE-trending (Figs. 3a, 4c, 6) and NW-trending (Fig. 3c, 4d, 6). The relative age of the two orthogonal sets is not well constrained, as only a few abutting relationships are found (Fig. 4d).

When considering the geometry of the orthogonal system at the scale of Yucca Mountain, some workers suggest that the two sets form a rectilinear pattern of joint swarms or clusters with swarm widths of 3 to 5 m and spacings between swarms of 150 to 200 m, based on anecdotal field observations (Barton et al., 1993, Sweetkind and Williams-Stroud, 1996). The present study attempts to resolve the importance of the orthogonal sets of tube-bearing joints in the overall fracture network by considering their orientations over areas of thousands of square meters as opposed to hundreds of square meters.

Timing of Tube-Bearing Joints and Volcanogenic Features

Tube-bearing joints at Yucca Mountain have two characteristics that we interpret to indicate that joint formation preceded lithophysae formation. First, tube-bearing joints very seldom intersect lithophysae, although lithophysae with decimeters diameters are common (Fig. 4a,c,d). If joint propagation occurred in the presence of lithophysae, intersections and terminations with lithophysae should occur (Barton et al., 1993; Buesch et al., 1996), partially because some joints should have also propagated toward existing lithophysae, in response to local stress perturbations around the expanding void (Kirsch, 1898; Lachenbruch, 1962). Second, some joint walls within about a centimeter of lithophysae show outward deformation by lithophysal inflation, so the walls are older.

Tube-bearing joints also have two features that we interpret to indicate that joint formation preceded tube formation. First, some tubes wrap through joint intersections, which indicates that these intersections are older. Second, tubes are only found on joint faces.

The millimeter-to-centimeter diameter tubes form anastomosing networks, which isolate areas of joint planes (Fig. 4b,d,e). Area edges match across tube walls, indicating the tubes dilated joint faces during their formation. A retrodeformation to remove the effects of tube formation (Fig. 4e) shows that tubes produced at least 15% vertical dilation of the joint face, accompanied by a few degrees of local rotation for some areas. This magnitude of vertical dilation is consistent with vertical expansion in the host unit of 16% to 22% due to lithophysal formation described by Barton et al. (1993) (Fig. 5). Thus, the tubes, which were degassing structures (Barton et al., 1993), were coeval with lithophysae formation. Since the tube-bearing joints are older than the lithophysae and the tubes, and gas pressure must exceed lithostatic for their inflation, the timeframe for their formation bounds the timing of joint development in a

lithophysae-free host. Thus, joint formation likely occurred within a month of tuff emplacement (Riehle et al., 1995).

Abundant vapor-phase silicates line the tube interiors and devitrification selvages commonly extend for half a tube diameter into the tuff matrix. In contrast, joint planes between tubes show only minor vapor-phase mineralization and very limited amounts of devitrification into the joint walls (Fig. 4e). Tubes formed in response to vertical inflation of the tuff as a result of degassing (Fig. 5). Once formed, the tubes received the initial flush of hot gas, from which there was rapid vapor-phase precipitation. Further cooling permitted escape of the less saturated gas vertically along the fracture.

Structural Geometry of Tube-Bearing Joints

A sample area of 20,787 m^2 with about 15% exposure or 3162 m^2 was examined on Live Yucca Ridge at Yucca Mountain to characterize the contribution of the orthogonal joint system to the total fracture network (Fig. 6, 7). Subhorizontal tube-bearing joints are not exposed in this area, so their geometry is not considered.

Both fracture traces and limits of exposed rocks were mapped so as to consider the influence of the distribution and quantity of rock exposure on trace data distribution. The sample area is about two orders of magnitude larger than that used for the cleared pavements, such as P100 (214 m^2; Fig. 3a), which is within the new sample area (Fig. 7).

We used a real-time kinematic differential GPS (DGPS) (Novatel®) with resolution of ±2 cm horizontal and ±10 cm vertical (2 sigma error) to map the topography of Live Yucca Ridge, and to create a fracture trace map. Fracture positions were mapped using the GPS data collector's "feature tagging" option, where the position is "tagged" with a user defined

alphanumeric identifier. Fractures were tagged at their visible ends and at several points in-between if they exceeded a few meters in size. Fractures were sequentially numbered, and designated as either tube-bearing or lacking tubes. In addition, fracture orientations were input into the data collector. The tagged data points were then connected in a GIS to create a fracture-trace map. These data were downloaded to Arcview™ software to construct a map with a GIS database. Other field observations were measured and recorded using compasses, field notebooks and cameras.

To facilitate useful, but efficient data collection over such a large sample area, the minimum recorded fracture trace length (cutoff length) was 2 m, and the minimum exposed area mapped was approximately equal to a circle with a diameter of 2 m. The truncation limit is an order of magnitude larger than the 0.2 m limit used to survey fracture traces on pavements such as P100 (Barton et al., 1993). The reasons for using the larger truncation limit in our study were that both previous work and our reconnaissance mapping indicated that tube-bearing joints dominantly have tracelengths greater than 2m, previous pavement work (Barton et al., 1993) provided sample sets for the geometry of smaller fractures, and previous investigations at Yucca Mountain documented the tremendous increase in time necessary to document patterns for tracelengths of less than 1m accurately (Sweetkind and Williams-Stroud, 1996).

The south side of Live Yucca Ridge is better exposed than the north, which is typical of the slopes of the east-west trending ridges at Yucca Mountain. While P100 and the related swarm of NE-trending tube-bearing joints are in a relatively well-exposed portion of the ridge, visual inspection of the mapped locations of tube-bearing joints shows that their abundance does not correlate to areas of best exposure (Fig. 7).

The true maximum length of tube-bearing joints is difficult to ascertain because their trace lengths are so long that they exceed the dimensions of even the largest exposures, and hence are censored (Epstein, 1954; Priest, 1993; Mauldon et al., 2001). In a few cases, fracture traces were dug out between exposures to partially overcome the effects of censoring and determine maximum trace length. These traces are visible as black lines that are mostly not contained in regions of exposure in Figure 7. Even with these efforts, true fracture tips were seldom found for tube-bearing joints, and we are restricted to saying that many tube-bearing joints have trace lengths exceeding 10 to 15m.

The two sets of tube-bearing joints have different trace distribution patterns. NE-trending traces are generally longer (apparent mean trace length of 4.1 m vs. 3.6 m), are either grouped in narrow swarms (locations A and B, Fig. 7) or occur as a few joints in near alignment (locations C and D, Fig. 7). In contrast, NW-trending tube-bearing joints occur in wider swarms and have traces that are more typically en echelon rather than co-linear (locations E and F, Fig. 7). Also, NW-trending joints are less numerous (67 vs. 126) than NE-trending joints (locations A and B, Fig. 7 and Fig. 8a).

The two sets of swarms form an approximately rectilinear network of fracture traces (Fig. 7) as described by Barton et al. (1993). The orthogonal distance between the two well-developed NE-trending joint swarms is about 150 m (Barton et al., 1993), however, this value is probably an overestimate of the swarm spacing, because between the two well developed NE-trending swarms are two poorly developed swarms, particularly around location C (Fig. 7), yielding a minimum swarm spacing of about 50 m for the NE-trending set. The NW-trending swarms also have spacings of about 50 m.

Tube-bearing joints have a greater cumulative trace length with a narrower orientation spectrum than joints without tubes (Fig. 7, 8). Even with censoring, field observations demonstrate that traces of tube-bearing joints, particularly NE-trending ones are longer than the traces of joints without tubes, and that tube-bearing joints are more numerous. Thus, the swarms of tube-bearing joints provide a rectilinear framework to the fracture network, while joints without tubes enhance fracture network connectivity.

Fumarolic Association for Tube-bearing Joints

Many pyroclastic deposits have early-formed joints (e.g., Sheridan, 1970; Hildreth, 1983; Keith, 1991), and near-orthogonal joints in tuffs have previously been recognized (Keith, 1991). Early-formed joints in the Valley of Ten Thousand Smokes and Bishop Tuff (Hildreth, 1983; Keith, 1991; Sheridan, 1970) are associated with fumarolic degassing and have obvious gas-escape features such as mineralized ridges at the top of the deposit and vapor-phase alteration of joint walls. These fumarolic joints have not been reported with tubes, but neither have they been investigated in units with lithophysae (e.g., Sheridan, 1970; Hildreth, 1983; Keith, 1991). Fumarolic joints in these analog pyroclastic deposits occur along ridges that are underlain by single long joints or narrow swarms of joints (see Figure 3a in Sheridan, 1970), which is consistent with the geometry of the tube-bearing joints at Yucca Mountain. Fumarolic joints provide the vertical pathway for gas escape during tuff compaction and welding, and their host ridges have lengths from as little as 10's of meters to greater than a kilometer. As a result, the underlying swarms of fumarolic joints would have the same lateral persistence as the ridges, which is a persistence shared by the tube-bearing joints at Yucca Mountain. Fumarolic joints formed during ridge construction are driven both by thermoelastic contraction as would be

expected for simple cooling joints (Engelder and Fischer, 1996) and by elevated fluid pressure (Secor, 1968) due to degassing. Given that tube-bearing joints at Yucca Mountain are geometrically similar to fumarolic joints, are the oldest joints, and formed in a lithophysae-free matrix, we interpret them to have been very early gas escape pathways, that may have served as the plumbing system for fumaroles at the surface.

Possible Stress Sources for Developing Subvertical Tube-bearing Joints

Because the Tiva Canyon Tuff was deposited in a region undergoing east-west extension (Zoback et al., 1981; Sawyer et al., 1994; Morris et al., 1996), and assuming that the orthogonal joints are mode I extension fractures with wall-normal displacements, they might be expected to strike N and E. However, across much of the Yucca Mountain region, the two tube-bearing sets strike NE and NW (Figs. 3, 6, 7, 8). Thus, at least one additional stress component other than the remote regional stresses must have operated to perturb the stress field from the regional stress state. Such stress perturbation might result from cooling-related effects, caldera evacuation during eruption, or active normal faulting due to regional stresses or related to the caldera evacuation and tuff deposition.

During tuff cooling, temperature gradients are greater vertically than horizontally. This vertical temperature gradient, and consequent differential thermal contraction, may explain the formation of sub-horizontal joints (Lachenbruch, 1962). While they could not be driven by tension related to the vertical temperature gradient, the formation of the subvertical joints could be partially explained by horizontal temperature gradients, although one might not expect them to be uniform in direction across a region. As a result, an additional stress component is needed.

Another cooling-related effect is differential compaction where thicker tuff deposits remain hotter for longer periods and compact more than thin deposits because of their higher total heat capacity. This creates a lateral stress gradient. For example, one set of fumarolic ridges in a system of orthogonal ridges in the Valley of Ten Thousand Smokes, Alaska was interpreted to form in response to differential compaction during cooling of the tuff (Keith, 1991). As the tuff deposit cooled, tuff in the valley center compacted more than the margins, creating tensional structures parallel to these margins. In another example for the general case of a simple basin, Sheridan (1970) proposed that vertical joint formation could be driven by differential compaction between the depocenter (thick deposits, more compaction) and the basin margins (thin deposits, less compaction) (Sheridan, 1970). For the Tiva Canyon Tuff at Yucca Mountain, if the depocenter of a NW-trending basin existed just to the north of the study area (Fridrich, 1999), the steepest compaction and temperature gradient would be along the short axis of the basin toward the depocenter. So, the greatest cooling-generated tension would be oriented NE-SW and would possibly generate NW-trending vertical joints.

The eruption of the tuff that formed the Tiva Canyon Tuff involved collapse of the Claim Canyon Caldera that ejected about 1000 km^3 of material from a site about 5 km north of the present study area (Fig. 1b; Byers et al., 1976a; Sawyer et al., 1994). Such a collapse would have perturbed the regional stress field directly, and possibly could have triggered movement on nearby normal faults (e.g., Nostro et al., 1998). Volcanic eruptions with less than 1% of this eruption volume have been interpreted to be causally linked to earthquakes on normal faults in regions with active extension (e.g., Abe, 1992; Nostro et al., 1998, and references cited within). The timespan of this link is typically 1 to 10 years between the two events, but could be much shorter for a larger event.

The major normal faults in the Yucca Mountain region were active within the 100,000 years before and during the million years after the deposition of the Tiva Canyon Tuff in response to regional extension in the central Basin and Range province (Christiansen et al., 1977; Sawyer et al., 1994; Day et al., 1998a, Fridrich, 1999). Thus, regional tectonic stresses with or without perturbation from the aftermath of caldera formation could have reasonably triggered normal faulting during cooling of the tuff. If one or more of the normal faults in the area slipped, the regional stress field would be locally perturbed, which could explain an orthogonal joint geometry that did not match horizontal stress directions for the regional stress field alone (e.g., Crider and Pollard, 1998; Katterhorn et al., 2000).

Ideally, one would like to quantitatively test these possibilities individually and together. However, lack of data, limited understanding of the material behavior of cooling tuffs, and a lack of robustness of current mechanical models to handle some of these possibilities, preclude the ideal approach. The role of differential compaction and thermal gradients cannot be tested, owing to the paucity of data about tuff thickness, possible basin geometry, and lateral temperature variations during cooling. Analytical models have been developed for modeling stress perturbation around small volume eruptive columns, but not for stress field perturbation effects of very large volume (ca. 1000 km^3) eruptions. However, the available data for the orientation and distribution of tube-bearing joints, for normal fault geometry, and for possible regional stress conditions during the Miocene at Yucca Mountain, do allow us to test whether interacting normal faults could locally perturb the regional stress field sufficiently to account for the formation of the swarms of fumarolic tube-bearing joints.

NORMAL FAULTING AND PERTURBATION OF REGIONAL STRESS FIELD

We use Poly3D to test the proposition that active faulting during cooling of the Tiva Canyon Tuff could have locally perturbed the stress field to produce orthogonal joint systems with orientations different from those expected from the Miocene regional stress field. Poly3D (Thomas, 1993) is a three-dimensional, boundary-element method computer code that calculates the stress and deformation fields around discontinuities in an elastic medium.

Model Configuration

We model three major faults near the fracture-map study area: the Solitario Canyon fault, the Paintbrush Canyon fault, and the northern segment of the Bow Ridge fault (Fig. 9). Because our interest is in very-near-surface phenomena, we model only the upper (planar) portions of the faults. Each fault is modeled as a planar rectangular discontinuity, subdivided into as many as 324 rectangular elements. The modeled Solitario Canyon fault strikes north, dips 75° W and has a trace length of 16 km. The modeled Paintbrush Canyon fault has parallel strike and dip and is slightly longer, at 19 km. The modeled northern segment of the Bow Ridge fault strikes 010° and dips 60°W. It has a trace length of 6 km. All three faults intersect the free surface of the model and extend 6 km down dip. The model fault geometries are simplified from the observed for numerical efficiency, and so that we may focus on the generalized effects of stress perturbation by faulting, rather than local effects of bends and steps in the fault traces.

The faults are imbedded in a homogeneous elastic half-space, with standard crustal rheology (Poisson's ratio = 0.25, shear modulus = 30 GPa). Although we expect cooling Tiva Canyon Tuff to be significantly less stiff, it represents only a small volume of the crustal section. In addition, model trials with order-of-magnitude variations in shear modulus show significant

changes in fault slip, but no changes relative to each other in the orientation of the local stress directions. Frictional resistance to slip is not modeled, but the effect of linearly increasing lithostatic (confining) stress with depth is included.

Although we do not have direct measurements of the stress state in the Miocene, we assume that deformation occurred in a normal-faulting stress regime, with maximum principal compressive stress (σ_1) vertical, intermediate principal compressive stress (σ_2) N-S, and minimum principal compressive stress (σ_3) E-W. This assumption is consistent with geologic estimates of Miocene stress state as interpreted by Zoback et al. (1981). We test magnitudes for S_h (minimum horizontal compressive stress) and S_H (maximum horizontal compressive stress) in the range of modern measurements at Yucca Mountain. Stock et al. (1985) give estimates for principal stresses, corrected for fluid pressure (Ferrill et al., 1999b), at 1 km depth as: S_V = 21 MPa, (approximately lithostatic), S_H = 17 MPa (or 4MPa less than lithostatic), and S_h = 11 MPa (or 10 MPa less than lithostatic).

Here we evaluate results for two model trials that differ in the assumptions for tectonic driving stresses. Inputs for tectonic driving stresses are defined in terms of differential stress values in principal planes of the stress tensor. In the context of these model inputs, positive normal stress is referred to as tension (following the convention of Crider and Pollard, 1998). These model inputs do not necessarily represent tensile tectonic stress in the earth's crust. In the first trial, fault slip is modeled as driven by 10 MPa east-west tension only, which simulates a differential stress of 10 MPa in the plane containing S_h and S_V. This boundary condition mimics a S_h of 10 MPa less than lithostatic load in the east-west direction, such that $S_h<S_H=S_V$, and $S_H=S_V$= the lithostatic stress. In the second trial, we also reduce the north-south horizontal stress (by 8 MPa), such that S_h + 10 MPa = S_H + 8 MPa = S_V. In this case, fault slip is modeled as

driven by an E-W tension in the model of 10 MPa and a N-S tension in the model of 8 MPa. This boundary condition mimics a S_h of 10 MPa less than lithostatic load in the east-west direction and a S_H of 8 MPa less than lithostatic load in the N-S direction.

Model Results and Interpretation

With these boundary conditions, the three modeled faults slip simultaneously, with maximum dip-slip at the free surface and approximately at the center of the fault trace. Slip distribution along each fault is approximately elliptical, modified by interaction among the three faults. The modeled segment of the Bow Ridge fault also shows a small component of left-lateral slip. The mean dip-slip on each fault is slightly more than 1 m. The modeled situation corresponds to a cluster of moderate-sized (Mw ~6) earthquakes, such as is common in western North America, for example the 1993 Klamath Falls, Oregon, earthquakes (Braunmiller et al., 1995), the Ridgecrest, California, sequence (Hauksson et al., 1995), or the much larger Dixie Valley-Fairview Peak, Nevada, sequence (Doser, 1986).

Vertical tensile fractures are expected to form perpendicular to the least horizontal stress (S_h). Figure 10a shows modeled orientations of S_h from which expected fracture orientations can be inferred for trial 1 (E-W only driving stress). A dominant N-S fracture pattern, perpendicular to the regional S_h, is seen away from faults and outside the region of fault overlap. In the region of overlap, local perturbation of the stress orientations, and consequent rotation of predicted fracture orientations, is observed. The joint orientation that is perpendicular to the predicted direction for the minimum horizontal stress compares favorably with the pattern of joint orientations recorded by Throckmorton & Verbeek (1995) (Fig. 6). A NE-trending set is predicted in the central block where the major clusters of tube-bearing joints occur (Fig. 6, 7,

10b), and a N-S trending set is predicted and found in the footwall of the Paintbrush Canyon fault. The strike of the modeled fracture orientations is not as easterly as the observed joints in the central block with a spread of orientations between 000° and 030° (Fig 10c).

In trial 2, we allow north-south reduction in the lithostatic load and the match between modeled fractures and observed joint orientations is improved (Fig. 11). The stress perturbation in the footwalls of both the modeled Solitario Canyon and Paintbrush Canyon faults is greater than in trial 1. The modeled fracture orientations in the vicinity of the study area on Live Yucca Ridge are a close match to the present-day joint trends with a range of 026° to 066° and a mode between 045° and 050°.

Our model results show that slip on faults can generate local stress perturbations that are consistent with joint orientations observed at Yucca Mountain. Thus, active faulting synchronous with the eruption of the Tiva Canyon Tuff is a plausible mechanism for the control of the orientation and distribution of tube-bearing joints within the tuff.

FORMATION OF NW-TRENDING JOINT SWARMS

Assuming that the NE-trending set of tube-bearing joints in the Tiva Canyon Tuff was formed during volcanic degassing and active normal faulting, what was the mechanism that formed the second orthogonal set with the necessary 90° rotation of the horizontal stress directions? The likely possibilities are a regional-scale rotation of stress directions, changes in displacement behavior of the normal faults, and more local-scale rotation due to formation of the first-formed NE-trending joints. Any of these mechanisms could have been aided by differential compaction in the postulated NW-trending basin.

Considering regional-scale rotation, the central Basin and Range in which Yucca Mountain lies, experienced E-W extension prior to 10 Ma (Zoback et al., 1981). Previous work (Zoback et al., 1981; Wernicke, 1992; Axen et al., 1993) does not indicate that a change occurred in regional principal strain directions and hence, regional principal stress directions during this E-W extension. Consequently, we discount the possibility of a regional-scale rotation of tectonic stresses.

Considering displacement behavior on the normal faults, horizontal stress directions might switch if fault-slip directions changed significantly or if different faults or parts of faults slipped sequentially. Although conceivable that changes in fault slip direction during a slip event or sequential slip on different faults or parts of faults could produce both the NW and NE-trending tube-bearing joints, diagnostic evidence for these scenarios is lacking for the joint system under investigation. We cannot, however, discount this possibility.

The possibility of a locally controlled rotation due to an additional perturbation of the stress field by the formation of the NE-trending joints remains. A geometric support for this possibility is the fact that the NE-trending joint swarms are better developed than the NW-trending swarms in terms of joint size and abundance within swarms. The better development of the older set is a typical feature of orthogonal joint systems formed by local stress release (Hancock, 1985; Caputo, 1995; Bai et al., 2001).

The case for local control of the rotation of the stress directions is analogous to the formation of stratal-bound layer-normal joints forming in response to remote tension (Hobbs, 1967; Gross et al., 1995). In this case, joint formation perturbs the stress field by causing a stress drop or shadow. Recent work by Bai et al. (2001) shows that when joint spacing of the older joint set is <1.7 times the thickness of the layer containing the joints, and when $S_h/S_H > 0.2$, the

horizontal stress directions in the rock mass between the first-formed joints swap. Given an interpreted penetration depth for the NE-trending joints of 20 to 30 m, which is the thickness of the upper lithophysal unit, and a swarm spacing of about 50 m, the spacing to thickness ratio in the Tiva Canyon Tuff is 2.5 to 1.6, and is about the critical threshold of 1.7 for stress swapping when the ratio of horizontal stresses >0.2, which seems likely in this case. Thus, a second perturbation of the stress field in the vicinity of Live Yucca Ridge by the formation of swarms of NE-trending tube-bearing joints is a possible mechanism for rotating the horizontal stress directions to allow the formation of NW-trending joints.

Care should be taken in applying this analogy to orthogonal swarm formation at Yucca Mountain. The analogous case is applied to fracture networks of individual joints in brittle rocks with spacings on the order of centimeters to meters, whereas the Yucca Mountain case considers swarms of joints on the scale of tens of meters that developed in a cooling but hot tuff with a more complex material behavior. The analogous case relies on uplift and erosion to achieve near surface conditions for formation of the cross joints, whereas at Yucca Mountain the process occurs quite close to the ground surface after minimal burial. Also, while joint formation at Yucca Mountain is partially driven externally by thermoelastic contraction due to cooling, the joint formation is also internally driven by fluid pressure generated by volcanic gases, which differs from the analogy. Still, the analogy does offer an explanation, future numerical modeling will explore the possibility of extrapolating this explanation to the larger-scale case of joint swarms partially driven by internal fluid pressure. Such an analysis would be applicable to sedimentary rocks with elevated fluid pressures in either the case of joints formed contemporaneously with fault displacements or in the absence of such displacement. In fact, the fluid-driven case may offer an explanation for some cases of joint swarm development, which is

a widely recognized phenomenon (e.g, Hancock, 1985; Pollard & Aydin, 1988, Odling et al., 1999).

DISCUSSION

Cooling Joints without Tubes

Cooling joints are ubiquitous features in moderately to densely welded tuff deposits (e.g., Smith et al., 1960; Ross and Smith, 1963; Cas and Wright, 1987). They form in response to tensional stress induced by thermal contraction during cooling (Lachenbruch, 1962; DeGraff and Aydin, 1987; Engelder and Fischer, 1996), and are not associated with ductile deformation features such as tubes or lithophysae (Enlows, 1955; Ross and Smith, 1963; Sheridan, 1970; Cas and Wright, 1987). Cooling joints are pseudo-columnar, smooth or curviplanar; lack bleached walls; occur in a variety of orientations; and vary in length between 1 to 15 meters. They also occur in tuffs with fumarolic joints, and terminate against those early-formed joints (e.g., Sheridan, 1970).

By analogy with other welded tuffs, abundant cooling joints should be expected in the rock volumes between early-formed fumarolic joints at Yucca Mountain (e.g., Sheridan, 1970). The characteristics of cooling joints in tuffs appear identical to the criteria used by previous workers to identify tectonic joints at Yucca Mountain (Morgan, 1984; Barton et al., 1984; Barton and Larsen, 1985; Carr, 1992; Barton et al., 1993, Sweetkind et al., 1995a, 1995b; Throckmorton and Verbeek, 1995; Albin et al., 1997; Eatman et al., 1997; Mongano et al., 1999). Given the morphological similarities and the reasonable expectation that the tube-bearing joints are not the only cooling joints in the tuff, we believe that many joints previously interpreted as tectonic joints at Yucca Mountain are likely cooling joints. Distinguishing between the origins of these

morphologically similar joints may require detailed studies of the different deuteric facies within the Tiva Canyon Tuff (cf. Buesch et al., 1996), because cooling joint attributes should exhibit a correlation with degree of degassing, welding, and devitrification processes.

Implications for Other Tuffs with Tube-bearing Joints at Yucca Mountain

The focus of this paper is on jointing in the upper lithophysal zone of the crystal poor member of the Tiva Canyon Tuff. The observations, interpretations, and conclusions, however, have direct relevance to fracturing in other parts of the Tiva Canyon and Topopah Spring Tuffs. The best data set available for evaluating the distribution and characteristics of fractures within Yucca Mountain are the scanline and full-periphery mapping data from the ESF and ECRB tunnels (Mongano et al., 1999; CRWMS M&O, 1998, 2000). Tube-bearing joints are also common in the Topopah Spring Tuff of the Paintbrush Group sampled in the underground ESF and ECRB tunnels at Yucca Mountain. The interpretation of very early origin (within days or weeks after pyroclastic deposition) for tube-bearing joints also applies to this separate cooling unit of the Paintbrush Group on the basis of a similar fracture morphology. Also, the interpretation that many of the joints without tubes that were previously interpreted to be tectonic may be cooling-related, also applies to the Topopah Spring Tuff.

During fracture data collection from the ESF and ECRB, cooling joints were identified based on the presence of tubular structures, and in the absence of tubular structures, on the basis of length >5m, smooth surfaces, presence of vapor-phase mineralization, vapor-phase margin, and undulatory surfaces. Tubular structures are generally associated with cooling joints in lithophysal units. Small-diameter tubes or no tubes on large, smooth planar or undulatory joints, and evidence of vapor phase mineralization or alteration are typical of less lithophysal or

lithophysae barren cooling units. Orientation data from cooling joints classified according to these criteria reveal that cooling joints through both the Tiva Canyon and Topopah Spring welded tuffs dominantly have northwest strikes. A secondary NE trending population is also present in the data (Mongano et al., 1999).

An approximately 1 km long intensely fractured zone was discovered during excavation of the north-south main drift of the exploratory studies facility. This zone of closely spaced fractures is overwhelmingly dominated by NW trending cooling joints (Mongano et al., 1999). The dominant cooling joint orientation at the northern end of the intensely fractured zone is NW, and cooling joint orientations gradually transition to WNW-ESE to the south. Mongano et al. (1999) illustrated that the intensely fractured zone corresponds to a large displacement gradient along the Ghost Dance fault. This correspondence between cooling joints and displacement gradient on the Ghost Dance fault implies that the Ghost Dance fault slipped during cooling of the Topopah Spring Tuff.

CONCLUSIONS

1. The oldest joints in the welded Tiva Canyon Tuff at Yucca Mountain are tube-bearing and consist of two orthogonal sets. They were previously interpreted to be related to tuff degassing and dilation during cooling. Given that such processes likely occurred within one month of tuff deposition, we believe that the entire orthogonal joint system formed within that timeframe.

2. Our proposed interpretation for the formation history of tube-bearing joints is consistent with field data and model results:

- Initial pyroclastic eruption of the Tiva Canyon Tuff and collapse of the Claim Canyon caldera;
- Deposition of the tuff over topography that may have included a shallow NW-trending basin;
- Development of a perturbed stress field due to a combination of (1) thermal gradient, (2) differential compaction, (3) caldera collapse, and (4) faulting;
- Slip on the Solitario Canyon, Bow Ridge, and Paintbrush Canyon faults, perhaps triggered by caldera collapse and increased vertical loading associated with newly deposited tuff sheet is a strong candidate for perturbing the regional stress field;
- Formation of the NE-trending joints as part of a set of fumarolic ridges in response to gas pressure with orientation controlled by the perturbed stress field;
- Formation of the NW-trending joints as part of a set of fumarolic ridges controlled by a stress swap due to the presence of the extensive NE-trending joint swarms and possibly aided by differential compaction across the NW-trending basin; and
- Tube formation on both joint sets during degassing and lithophysae formation in the upper Tiva Canyon Tuff.

Modeling of fault-controlled stress field perturbation does not completely exclude other possible contributions to stress field perturbation due to either an absence of appropriate data or limitation in available modeling techniques. For example, with appropriate data, the roles of differential compaction and thermal gradients could be explicitly assessed. Similarly, a better understanding of the role of caldera collapse in perturbing stress fields

and triggering fault motions might provide a sufficient basis for a quantitative analysis of this possibility. Nonetheless, we believe that this contribution represents a useful first attempt to relate the roles of caldera collapse, tuff deposition, tuff cooling, fault behavior and joint development to explain the origin of a joint network with a very interesting formation history. This interpretation also illustrates that a series of stress sources acting at a variety of scales, time spans and magnitudes can combine to produce an apparently simple orthogonal fracture geometry.

3. Because previous work had identified the tube-bearing joints as the cooling joints, this new interpretation implies that some joints previously identified as having a tectonic origin are cooling joints that lack tubes and formed in response to thermoelastic contraction.

4. Our conclusions regarding very early development of joints with tubular structures, and the possibility that some of the interpreted tectonic joints are actually contractional cooling joints, apply to joints with similar tubular structures throughout the Paintbrush Group. Strong orientation clustering of interpreted cooling joints, and common occurrence of NW and NE strike trends indicate that stress field perturbation was a recurrent process during the deposition and cooling of two welded tuff units of the Paintbrush Group.

ACKNOWLEDGMENTS

This paper was prepared to document work performed by the Center for Nuclear Waste Regulatory Analyses (CNWRA) for the U.S. Nuclear Regulatory Commission (NRC) under Contract No. NRC-02-97-009. The activities reported here were performed on behalf of the NRC Office of Nuclear Material Safety and Safeguards, Division of Waste Management. The report is an independent product of the CNWRA and does not necessarily reflect the views or regulatory position of the NRC. We thank James P. Hogan for assistance in the field, and Rebecca Emmot for assistance with manuscript preparation. Critical reviews by James P. Evans, Philip Justus, Wesley C. Patrick, and Larry McKague greatly improved the manuscript.

REFERENCES CITED

Abe, K., 1992, Seismicity of the caldera-making eruption of Mount Katmai, Alaska in 1912: Bulletin of the Seismological Society of America, v. 82, p. 175–191.

Albin, A.L., Singleton, W.L., Moyer, T.C., Lee, A.C., Lung, R.C., Eatman, G.L.W., and Barr, D.L., 1997, Geology of the Main Drift – Station 28+00 to 55+00, Exploratory Studies Facility, Yucca Mountain Project, Yucca Mountain, Nevada: Summary Report by the United States Bureau of Reclamation to the United States Department of Energy, DTN GS970208314224.005.

Axen, G.J., W.J. Taylor, and J.M. Bartlet, 1993, Space-time patterns and tectonic controls of Tertiary extension and magmatism in the Great Basin of the western United States: Geological Society of America Bulletin, v. 105, p. 56–76.

Bai, T., Maerten, L., Gross, M.R., and Aydin, A., 2002, Orthogonal cross joints: Do they imply a regional stress rotation?: Journal of Structural Geology, v. 24, p. 77-88.

Banks, N.G., and Hoblitt, R.P., 1981, Summary of temperature studies of 1980 deposits, *in* Lipman, P.W., and Mullineaux, D.R., ed., The 1980 Eruptions of Mount St. Helens, Washington: U.S. Geological Survey Professional Paper, v. 1250, p. 295–314.

Barton, C.C., Howard, T.M., and Larsen, E., 1984, Tubular structures on the faces of cooling joints – A new volcanic feature: Eos, Transactions of the American Geophysical Union v. 65, p. 1148.

Barton, C.C., and Larsen, E., 1985, Fractal geometry of two-dimension fracture networks at Yucca Mountain, *in* Stephanson, O., ed., Proceedings of the International Symposium on Fundamentals of Rock Joints, Sweden, Centek Publishers, p. 77–84.

Barton, C.C., Larsen, E., Page, W.R., and Howard, T.M., 1993, Characterizing fractured rock for fluid-flow, geomechanical, and paleostress modeling: Methods and preliminary results from Yucca Mountain, Nevada: United States Geological Survey Open-File Report, 93–269.

Bierwirth, P.N., 1982, Experimental Welding of Volcanic Ash [B.S. Honors Thesis]: Australia, Monash University.

Buesch, D.C., Beason, S.C., and Spengler, R.W., 1999, Relations among welding, vapor-phase activity, crystallization, and fractures in the Tiva Canyon and Topopah Spring tuffs, at Yucca Mountain: Geological Society of America Abstracts with Program, v.31, p. A476-477.

Buesch, D.C., Spengler, R.W., Moyer, T.C., and Geslin, J.K., 1996, Proposed Stratigraphic Nomenclature and Macroscopic Identification of Lithostratigraphic Units of the Paintbrush Group Exposed at Yucca Mountain, Nevada: United States Geological Survey Open-file Report, 94–469.

Braunmiller, J., Nblek, J. Leitner, B., and Qamar, A., 1995, The 1993 Klamath Falls, Oregon, earthquake sequence: Source mechanisms from regional data: Geophysical Research Letters v. 22, p. 105–108.

Bursik, M.I., Woods, A.W., 1996, The dynamics and thermodynamics of large ash flows: Bulletin of Volcanology, v. 58, p. 175–193.

Byers, F.M. Jr., Carr, W.J., Orkild, P.P., Quinlivan, W.D., and Sargent, K.A., 1976, Volcanic Suites and Related Cauldrons of the Timber Mountain-Oasis Valley Caldera Complex, United States Geological Survey Professional Paper, v. 919.

Caputo, R., 1995, Evolution of orthogonal sets of extension joints: Terra Nova, v. 7, p. 479–490.

Carr, W.J., 1992, Structures in continuously cored, deep drill holes at Yucca Mountain, Nevada with notes on calcite occurrence: Sandia National Laboratories, SAND91–7037.

Cas, R.A.F., and Wright, J.V., 1987, Volcanic Successions: Unwin Hyman Inc., Winchester, MA.

Christiansen, R.L., Lipman, P.W., Carr, W.J., Byers Jr., F.M., Orkild, P.P, and Sargent K.A., 1977, Timber Mountain–Oasis Valley caldera complex of southern Nevada: Geological Society of America Bulletin, v. 88, p. 943–959.

CRWMS M&O (Civilian Radioactive Waste Management System Management and Operating Contractor), 2000, Fracture Geometry Analysis for the Stratigraphic Units of the Repository Host Horizon: ANL–EBS–GE–000006 REV 00. Las Vegas, Nevada.

CRWMS M&O, 1998, Geology of the Exploratory Studies Facility Topopah Spring Loop, BAB000000-0171-0200-00002,REV01, Las Vegas, Nevada.

Crider, J.G., and D.D. Pollard, 1998, Fault linkage: Three-dimensional mechanical interaction between echelon normal faults: Journal of Geophysical Research, v. 103(B10), p. 24,373–24,391.

Day, W.C., R.P. Dickerson, C.J. Potter, D.S. Sweetkind, C.A. San Juan, R.M. Drake, II, and C.J. Fridrich, 1998a, Geologic map of the Yucca Mountain Area, Nye County, Nevada: United States Geological Survey, Geological Investigations Series I–2627, Scale 1:24,000, 1 sheet.

Day, W.C., Potter, C.J., and Sweetkind, D., 1998b, Bedrock geologic map of the central block area, Yucca Mountain, Nye County, Nevada: United States Geological Survey Miscellaneous Investigation Series, Map I-2601, Scale 1:6000, 2 sheets.

DeGraff, J.M., and Aydin, A., 1987, Surface morphology of columnar joints and its significance to mechanics and direction of joint growth: Geological Society of America Bulletin, v. 99, p. 605–617.

Doser, D. I., 1986, Earthquake processes in the Rainbow Mountain-Fairview Peak-Dixie Valley, Nevada, region 1954–1959: Journal of Geophysical Research, v. 91, p. 12,572–12,586

Dunne, W.M., and North, C.P., 1990, Orthogonal fracture systems at the limits of thrusting: an example from southwestern Wales: Journal of Structural Geology, v. 12, p. 207–215.

Eatman, G.L.W., Singleton, W.L., Moyer, T.C., Barr, D.L., Albin, A.L., Lung, R.C., and Beason, S.C., 1997, Geology of the South Ramp – Station 55+00 to 78+77, Exploratory Studies Facility, Yucca Mountain Project, Yucca Mountain, Nevada. Milestone SPG42CM3: Denver, Colorado, United States Geological Survey.

Engelder, T., 1985, Loading path to joint propagation during cycle: an example to the Appalachian Plateau, USA. Journal of Structural Geology, v. 7, p. 459-476.

Engelder, T., and Fischer, M.P., 1996, Loading configurations and driving mechanisms for joints based on the Griffith energy-balance concept. Tectonophysics, v. 256, p. 253–277.

Enlows, H.E., 1955, Welded tuffs of the Chiricahua National Monument, Arizona: Geological Society of America Bulletin, v. 66, p. 1215–1246.

Epstein, B., 1954, Truncated life tests in the exponential case: Annals of Mathematics and Statistics, v. 25, p. 555.

Eyal, Y., and Reches, Z., 1983, Tectonic analysis of the Dead Sea rift region since the Late Cretaceous based on mesostructures: Tectonics, v. 2, p. 167–185.

Fabbri, O., Gaviglio, P., and Gamond, J.-F., 2001, Diachronous development of master joints of different orientations in different lithological units within the same fore-arc basin deposits, Kyushu, Japan: Journal of Structural Geology, v. 23, p. 239–246.

Ferrill, D.A., and Morris, A.P., 2001, Displacement gradient and deformation in normal fault systems: Journal of Structural Geology, v. 23, p. 619–638.

Ferrill, D.A., Stamatakos, J.A., Jones, S.M., Rahe, B., McKague, H.L., Martin, R.H., and Morris, A.P., 1996, Quaternary slip history of the Bare Mountain fault (Nevada) from the morphology and distribution of alluvial fan deposits: Geology, v. 24, p. 559–562.

Ferrill, D.A., Stamatakos, J.A., and Sims, D., 1999a, Normal fault corrugation: Implications for growth and seismicity of active normal faults: Journal of Structural Geology, v. 21, p. 1027–1038.

Ferrill, D.A., Winterle, J., Wittmeyer, G., Sims, D., Colton, S., Armstrong, A., and Morris, A.P., 1999b, Stressed rock strains groundwater at Yucca Mountain, Nevada: GSA Today, v. 9, n. 5, p. 1–8.

Flint, A.L., J.A. Hevesi, and L.E. Flint, 1996, Conceptual and Numerical Model of Infiltration for the Yucca Mountain Area, Nevada: U.S. Geological Survey Water Resources Investigation Report, Milestone 3GUI623M, Denver, Colorado, United States Geological Survey.

Flint, L.E., and A.L. Flint, 1995, Shallow infiltration processes at Yucca Mountain, Nevada–Neutron logging data 1984–93: U.S. Geological Survey Water-Resources Investigations Report, 95-4035, Denver, Colorado, United States Geological Survey.

Fridrich, C.J., 1999, Tectonic evolution of the Crater Flat basin, Yucca Mountain region, Nevada. Cenozoic Basins of the Death Valley Region: *in* Wright, L., and Troxel, B., eds. Geological Society of America Special Paper, v. 333, p. 169–195.

Friedman, I., Long, W., and Smith, R.L., 1963, Viscosity and water content of rhyolite glass: Journal of Geophysical Research, v. 68, p. 6522–6535.

Gross, M.R., 1993, The origin and spacing of cross joints: examples from the Monterey Formation, Santa Barbara Coastline, California. Journal of Structural Geology 15, 737-751.

Gross, M.R., Fischer, M.P., Engelder, T., and Greenfield, R.J., 1995, Factors controlling joint spacing in interbedded sedimentary rocks: integrating numerical models with field observations from the Monterey Formation, U.S.A, *in* Ameen, M.S., ed., Fractography: fracture topography as a tool in fracture mechanics and stress analysis: Geological Society of London Special Publication v. 92, p. 215–233.

Hancock, P.L., 1985, Brittle microtectonics: principles and practice: Journal of Structural Geology, v. 7, p. 437–457.

Hauksson, E., Hutton, K., Kanamori, H., Jones, L., Mori, J., Hough, S., and Roquemore, G., 1995, Preliminary report on the 1995 Ridgecrest earthquake sequence in eastern California, Seismological Research Letters, v. 66, p. 54–60.

Hildreth, W., 1983, The compositionally zoned eruption of 1912 in the Valley of Ten Thousand Smokes, Katmai National Park, Alaska: Journal of Volcanology and Geothermal Research, v. 18, p. 1–56.

Hobbs, D.W., 1967, The formation of tension joints in sedimentary rocks: an explanation: Geological Magazine, v. 104, p. 550–556.

Katterhorn, S.A., Aydin, A., and Pollard, D.D., 2000, Joints at high angles to normal fault strike: an explanation using 3-D numerical models in fault-perturbed stress fields: Journal of Structural Geology, v. 22, p. 1–24.

Keith, T.E.C., 1991, Fossil and active fumaroles in the 1912 eruptive deposits, Valley of Ten Thousand Smokes, Alaska: Journal of Volcanology and Geothermal Research, v. 45, p. 227–254.

Kirsch, G., 1898, Die theorie der elastizitat und die bedurfnisse der festigheitslehre: Zeitschrift des Vereines Deutscher Ingenieure. v. 42, p. 797.

La Pointe, P.R., Hudson, J.A., 1985, Characterization and interpretation of rock mass joint patterns: Geological Society of America Special Paper, v. 199, 37 p.

Lachenbruch, A.H., 1962, Mechanics of thermal contraction cracks and ice-wedge polygons in permafrost: Geological Society of America Special Paper, v. 70, 65 p.

Lipman, P.W., and Friedman, I., 1975, Interaction of meteoric water with magma: An oxygen-isotope study of ash-flow sheets from southern Nevada: Geological Society of America Bulletin, v. 86, p. 695–702.

Lofgren, G., 1971, Experimentally produced devitrification textures in natural rhyolitic glass. Geological Society of America Bulletin v. 82, p. 111–124.

Martel, S., 1994, On the paradox of systematic, contemporaneous, orthogonal opening-mode fractures, *in* Nelson, R., and Laubach, S., eds., Rock Mechanics. Rotterdam, Balkema, p. 801–808.

Mauldon, M., Dunne, W.M., and Rohrbaugh, M.R., 2001, Circular scanlines and circular windows: New tools for characterizing the geometry of fracture traces: Journal of Structural Geology, v. 23, p. 247-258.

Miller, T.F., 1990, A numerical model of volatile behavior in nonwelded cooling pyroclastic deposits: Journal of Geophysical Research, v. 95, p. 19,349–19,364.

Monsen, S.A., Carr, M.D., Reheis, M.C., and Orkild, P.P., 1992, Geologic map of Bare Mountain, Nye County, Nevada: United States Geological Survey Miscellaneous Investigations Series, Map 2201, 1:24,000 scale.

Mongano, G.S., Singleton, W.L., Moyer, T.C., Beason, S.C., Eatman, G.W., Albin, A.L., and Lung, R.C., 1999, Geology of the ECRB Cross Drift – Exploratory Studies Facility, Yucca Mountain Project, Yucca Mountain, Nevada: Milestone SPG42GM3. Denver, Colorado, United States Geological Survey.

Morgan, T.L., 1984, Fracture characterization in the Tiva Canyon Member, Paintbrush Tuff, Yucca Mountain [M.S. thesis], Fort Collins, Colorado, Colorado State University.

Morris, A.P., Ferrill, D.A., and Henderson, D.B., 1996, Slip tendency analysis and fault reactivation: Geology, v. 24, p. 275–278.

Nostro, C., Stein, R. S., Cocco, M., Belardinelli M. E., and Marzocchi, W., 1998, Two-way coupling between Vesuvius eruptions and southern Apennine earthquakes (Italy) by elastic stress transfer: Journal of Geophysical Research, v. 103, p. 24,487–24,504.

Odling, N.E., Gillespie, P., Bourgine, B., Castaing, C., Chiles, J-P., Christensen, N.P., Fillion, E., Genter, A., Olsen, C., Thrane, L., Trice, R., Aarseth, E., Walsh, J.J., and Watterson, J., 1999, Variations in fracture system geometry and their implications for fluid flow in fractured hydrocarbon reservoirs: Petroleum Geoscience, v. 5, p. 373–384.

Olson, J.E., 1996, Post-compressional relaxation and orthogonal fracture pattern development: Geological Society of America Abstracts with Programs, v. 28, n. 1, p. 56.

Pollard, D.D., and Aydin, A., 1988, Progress in understanding jointing over the past century: Geological Society of America Bulletin, v. 100, p. 1181–1204.

Priest, S.D., 1993, Discontinuity Analysis for Rock Engineering, New York, Chapman & Hall.

Ragan, D.M., and Sheridan, M.F., 1972, Compaction of the Bishop Tuff, California: Geological Society of America Bulletin, v. 83, p. 95–106.

Rawnsley, K.D., Peacock, D.C.P., Rives, T., Petit, J.-P., 1998, Joints in the Mesozoic sediments around the Bristol Channel Basin: Journal of Structural Geology, v. 20, p. 1641-1661.

Rawnsley, K.D., Rives, T., Petit, J.-P., Hencher, S.R., and Lumsden, A.C., 1992, Joint development in perturbed stress fields near faults: Journal of Structural Geology, v. 20, p. 1641–1661.

Riehle, J.R., 1973, Calculated compaction profiles of rhyolitic ash-flow tuffs. Geological Society of America Bulletin, v. 84, p. 2193–2216.

Riehle, J.R., Miller, T.F., and Baley, R.A., 1995, Cooling, degassing and compaction of rhyolitic ash flow tuffs: a computational model: Bulletin of Volcanology, v. 57, p. 319–336.

Rives, T., Rawnsley, K.D., Petit, J.-P., 1994, Analogue simulation of natural orthogonal joint set formation in brittle varnish: Journal of Structural Geology, v. 16, p. 419-429.

Rosenbaum, J.G., 1986. Paleomagnetic directional dispersion produced by plastic deformation in a thick Miocene welded tuff, southern Nevada: Implications for welding temperatures: Journal of Geophysical Research, v. 91, p. 12,817–12,834.

Rosenbaum, J.G., 1993, Magnetic grain-size variations through an ash flow sheet: Influence on magnetic properties and implications for cooling history: Journal of Geophysical Research, v. 98, p. 11,715–11,727.

Ross, C.S., and Smith, R.L., 1961, Ash-Flow Tuffs: Their Origin, Geologic Relations and Identification: United States Geological Survey Professional Paper, v. 366.

Sawyer, D.R., Fleck, R.J., Lanphere, M.A., Warren, R.G., Broxton, D.E., and Hudson, M.R., 1994, Episodic caldera volcanism in the Miocene southwestern Nevada volcanic field: Revised stratigraphic framework, $^{40}Ar/^{39}Ar$ geochronology, and implications for magmatism and extension: Geological Society of America Bulletin, v. 106, p. 1304–1318.

Scott, R.B., 1990, Tectonic setting of Yucca Mountain, southwest Nevada: Geological Society of America Memoir, v. 176, p. 251–282.

Scott, R.B., Bonk, J., 1984, Preliminary Geologic Map of Yucca Mountain, Nye County, Nevada, with Geologic Sections: United States Geological Survey Open-File Report, 84–494.

Secor, D.T., 1968, Mechanics of natural extension fracturing at depth in the earth's crust. In: Baer A.J. and Norris, D.K., eds., Proc. Conf. On Research in Tectonics, Ottawa 1968, GSC Paper 68-52, p. 3–48.

Sheridan, M.F. 1970, Fumarolic mounds and ridges of the Bishop Tuff, California: Geological Society of America Bulletin, v. 81, p. 851–868.

Smith, R.L., 1960, Zones and Zonal Variations in Welded Ash Flows: United States Geological Survey Professional Paper, v. 354-F.

Stauffer, M.R., and Gendzwill, D.J., 1987, Fractures in the northern plains, stream patterns and mid-continent stress field. Canadian Journal of Earth Science, v. 24, p. 1086–1097.

Stock, J.M., Healy, J.H., Hickman, S.H., and Zoback, M.D., 1985, Hydraulic fracturing stress management at Yucca Mountain, Nevada, and relationship to the regional stress field. Journal of Geophysical Research, v. 90, p. 8691–8706.

Sweetkind, D.S., Verbeek, E.R., Geslin, J.K., and Moyer, T.C., 1995a, Fracture character of the Paintbrush Tuff nonwelded Hydrologic Unit, Yucca Mountain, Nevada: United States Geological Survey Administrative Report.

Sweetkind, D.S., Verbeek, E.R., Singer, F.R., Byers, F.M., and Martin, L.G., 1995b, Surface fracture network at pavement P2001, Fran Ridge, near Yucca Mountain, Nye County, Nevada: United States Geological Survey Administrative Report.

Sweetkind, D.S., and Williams-Stroud, S.C., 1996, Characteristics of fractures at Yucca Mountain, Nevada: Synthesis Report: United States Geological Survey Administrative Report.

Thomas, A.L., 1993, Poly3D: A three-dimensional, polygonal element, displacement discontinuity boundary element computer program with applications to fractures, faults and cavities in the Earth's crust [M.S. thesis], Stanford CA, Stanford University.

Throckmorton, C.K., and Verbeek, E.R., 1995, Joint networks in the Tiva Canyon and Topopah Spring Tuffs of the Paintbrush Group, southwestern Nevada: United States Geological Survey, Open-File Report 95-2.

Ver Steeg, K., 1942, Jointing in coal beds of Ohio: Economic Geology, v. 37, p. 503–509.

Wernicke, B., 1992, Cenozoic extensional tectonics of the U.S. Cordillera, *in* Burchfiel, B.C., Lipman, P.W., and Zoback, M.L., eds., The Cordilleran Orogen: Conterminous United States. Geological Society of America, Geology of North America, v. G-3, p. 553–581.

Winograd, I.J., 1971, Hydrogeology of ash flow tuff: a preliminary statement: Water Resources Research, v. 7, p. 994–1006.

Zoback, M.L., Anderson, R.E., and Thompson, G.A., 1981, Cainozoic evolution of the state of stress and style of tectonism of the Basin and Range province of the western United States: Philosophical Transactions of the Royal Society of London, v. A300, p. 407–434.

Captions

Figure 1. (A) Geologic map of Yucca Mountain, Nevada. Map is based on geologic mapping of Day, et al. (1998a) and shows proposed repository outline, topographic contours, distribution of Tiva Canyon Tuff, Exploratory Studies Facility (ESF), Enhanced Characterization of the Repository Block (ECRB), and locations of Pavements 100, 200, and 300; and the Live Yucca Ridge fracture study area. (B) Regional map showing location of Yucca Mountain with respect to the caldera complexes to the north.

Figure 2. Generalized stratigraphic table for the tuffs of the Paintbrush Group and the overlying and underlying tuff units.

Figure 3. Fracture trace maps for cleared pavements in upper lithophysal zone of the crystal-poor member of the Tiva Canyon Tuff (after Barton et al., 1993). (A) Pavement 100; (B) Pavement 200; (C) Pavement 300 (modified from Barton et al., 1993). Pavement locations in Figure 1. Thick lines - tube-bearing joints, thin lines - other fractures, dashed line - perimeter of mapped pavement, medium gray regions - abundant small fracture traces, stippled regions - fracture faces, arrowhead symbol - North direction

Figure 4. Photographs of fractures in upper lithophysal unit of the Tiva Canyon Tuff: (A) Smooth cooling joint with tubular structures defines one face of loose block (right side of photo), and later joint (at approximately 90°) with rougher surface morphology cuts lithophysae (left side of photo); (B) tubular structures on cooling joint surface shown in (a); (C) cooling joint swarm on Pavement 100 (view toward the southwest); (D) intersection of two cooling joints on Pavement 100; (E) retrodeformation of tubes by matching sides to show volume increase during tube formation. Expanded part of photo

shows small-aperture fractures and large aperture tubes cutting one face of a cooling joint. Tubes and fracture tips have bleached walls. The expanded image shows fractures with apertures ranging from <1mm at fracture tips to nearly 1 cm along major tubes. Regardless of aperture, fracture walls show bleaching indicative of vapor-phase mineralization and alteration of wall rock. Unbleached areas away from tube fractures are part of the vertical joint that would have been forced tightly closed by lateral stress caused by gas expansion and formation of lithophysae.

Figure 5. Sequence of formation of cooling joints with tubes. (A) Contractional joint surface propagates through rock prior to the formation of lithophysae. (B) Cooling joint causes formation of adjacent brittle zone. As the rock expands vertically with the formation of lithophysae, sub-horizontal, tube-like fractures develop within the brittle zone. (C) Continued degassing of the rock utilizes these tube for gas flow. (D) An expanded view of a cooling joint to show that the two sides are mirror images of each other.

Figure 6. Map of Yucca Mountain to Fran Ridge region showing strikes of orthogonal tube-bearing joints (modified from Throckmorton and Verbeek, 1995), and the locations of Figures 1a and 7. Dots on joint trend tips are station locations.

Figure 7. Fracture trace map at Live Yucca Ridge, Yucca Mountain showing fracture traces and rock exposure. Topographic contour interval is 10 m, and location grid is the UTM Zone 11 NAD27 system. Letters in rectangles are locations referred to in the text.

Figure 8. Orientation data for joints on Live Yucca Ridge. Left column: Lower hemisphere, equal area plot of poles to joints. Middle column: Un-weighted rose diagram of joint traces. Plot radius = 20%. Right column: Length-weighted rose diagram of joint traces. Plot radius = 20%. (A) Tube-bearing joints; number of joints = 272; cumulative trace

length = 1069 m. (B) Joints without tubes; number of joints = 214; cumulative trace length = 737 m. (C) All joints; number of joints = 486; cumulative trace length = 1806 m.

Figure 9. 3D perspective view of modeled faults, view to the NE. Star is on the ground surface and marks the location of Live Yucca Ridge. Origin of coordinate system corresponds to UTM 550000, 4075000.

Figure 10. Modeled stress trajectories for the case of E-W tension = 10 MPA. Results for 100 m depth. First-formed joints would form perpendicular to arrows. (A) Regional view. Arrows show direction of minimum horizontal compressive stress, S_h. Perturbation is observed in the overlap zone between the faults. SCF=Solitario Canyon Fault. BRF=Bow Ridge Fault. PCF=Paintbrush Canyon fault. Broad grey line shows southern segment of BRF, not modeled. Narrow grey line is approximate location of the ESF. Star locates Live Yucca Ridge. Coordinate system as in Fig. 9. Box outlines area of B. (B) Details of the stress perturbation in the region around Live Yucca Ridge. Heavy lines are observed joint populations (Throckmorton and Verbeek, 1995). Deflection of S_h in between SCF and BRF is greatest north of the ESF. Box indicates data plotted in C. (C) Rose diagrams of expected first-formed joint orientations in the vicinity of Live Yucca Ridge. Range is from 000 to 030. Plot radius = 50%. (D) Angular mismatch between modeled stress trajectories and joint populations on and near Live Yucca Ridge.

Figure 11. Modeled stress trajectories for the case of E-W tension = 10 MPA and N-S tension = 8 MPA. Model results for 100 m depth. First-formed joints would form perpendicular to arrows. All symbols as in Fig. 10. (A) Regional view. Greater deflection is observed in the footwall of both the SCF and PCF. (B) Details of the stress perturbation in the region

around Live Yucca Ridge. (C) Rose diagrams of expected first-formed joint orientations in the vicinity of Live Yucca Ridge. Range is from 026° to 066° with a mode between 045° and 050.° (D) Angular mismatch between modeled stress trajectories and joint populations on and near Live Yucca Ridge.

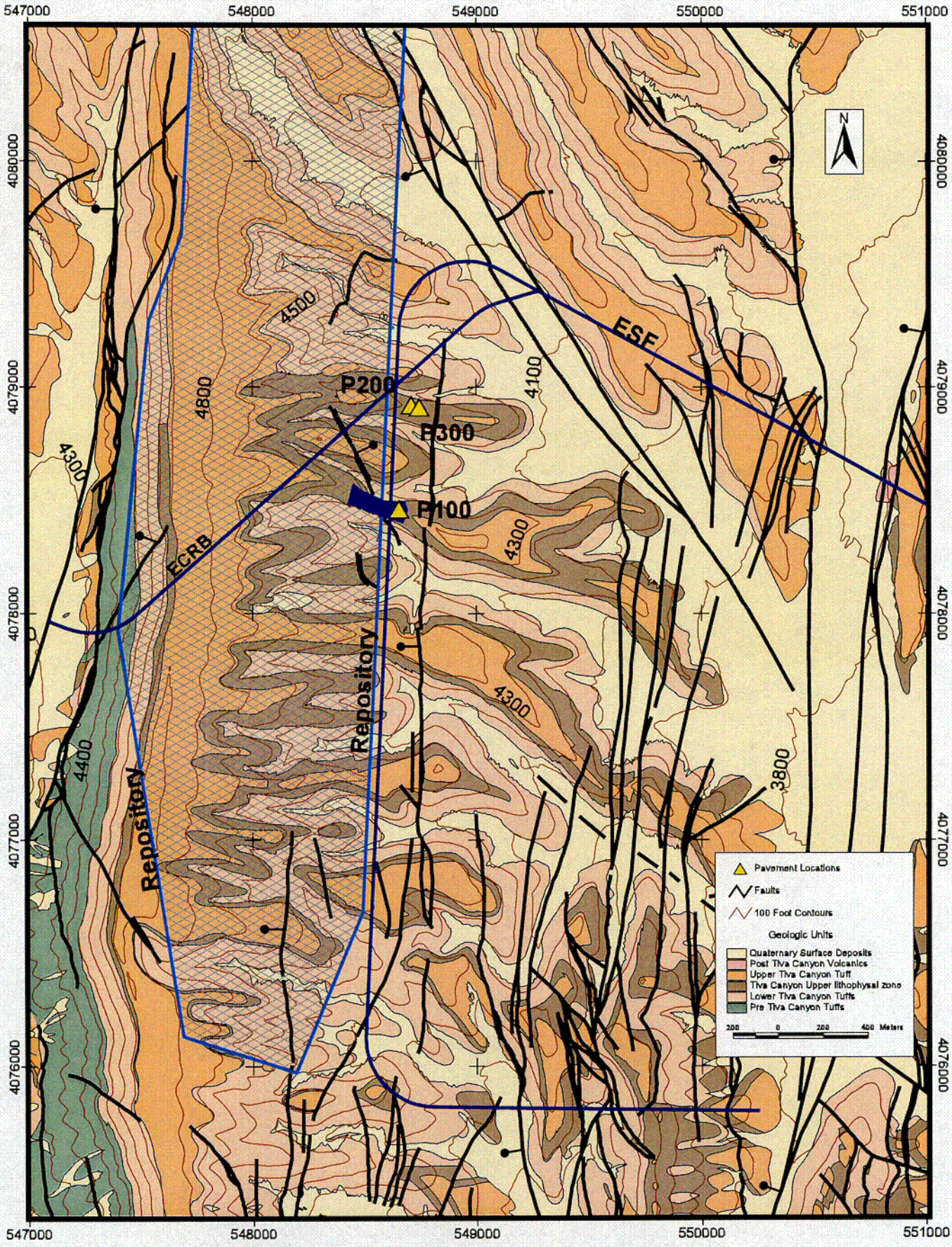

Fig. 1A
Dunne et al.

C01

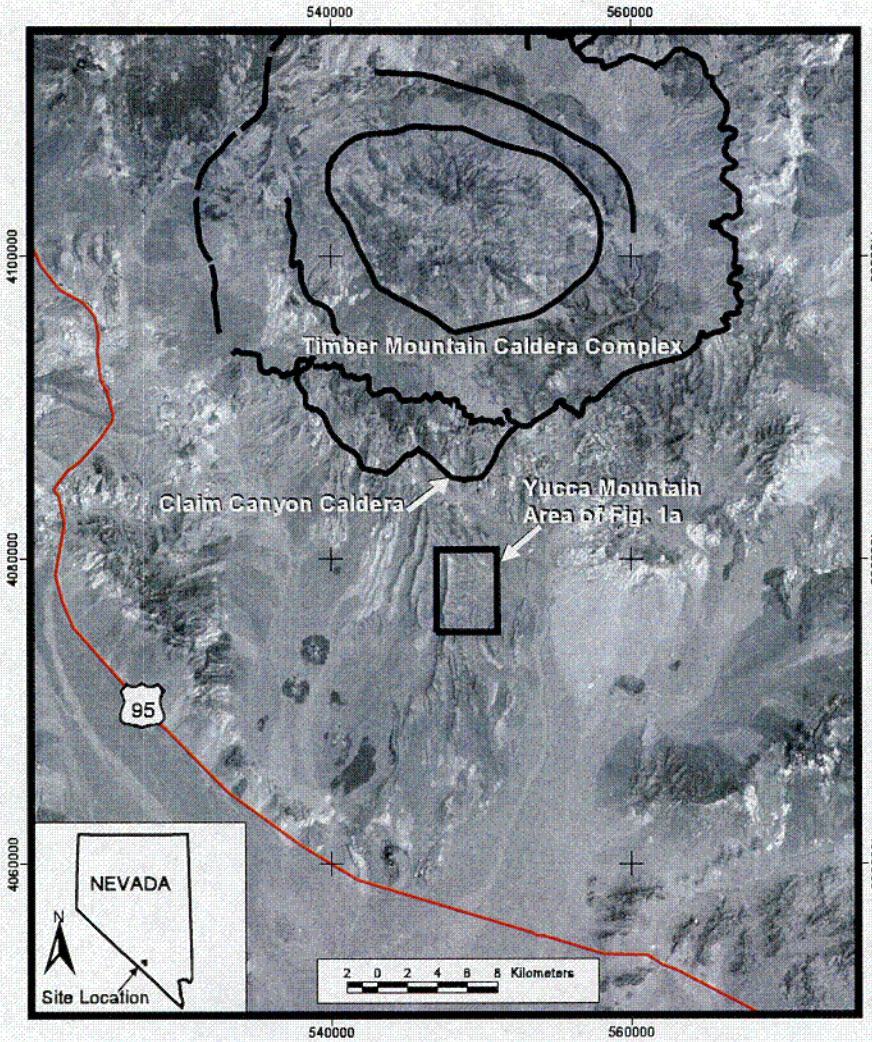

Fig. 1B
Dunne et al.

C02

GROUP	FORMATION	AGE
Timber Mountain Group	Rainier Mesa Tuff	11.6 Ma
Paintbrush Canyon Group	Bedded Tuff	
	Tiva Canyon Tuff	12.7 Ma
	Yucca Mountain Tuff	
	Pah Canyon Tuff	
	Topopah Spring Tuff	12.8 Ma
	Calico Hills Formation	12.9 Ma
Crater Flat Group	Prow Pass Tuff	
	Bullfrog Tuff	13.25 Ma
	Tram Tuff	>13.5 Ma

Fig. 2
Dunne et al.

(A)

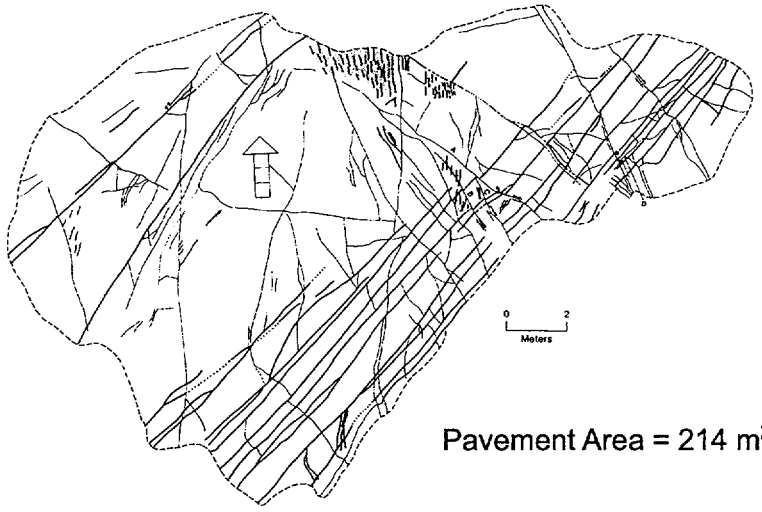

Pavement Area = 214 m^2

(B)

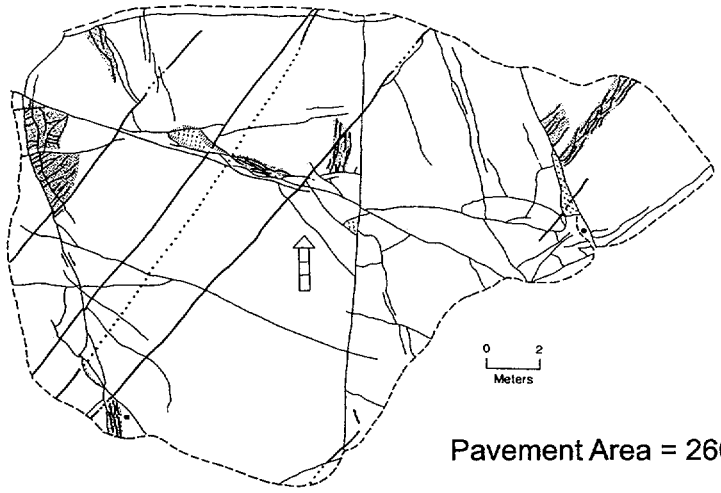

Pavement Area = 260 m^2

(C)

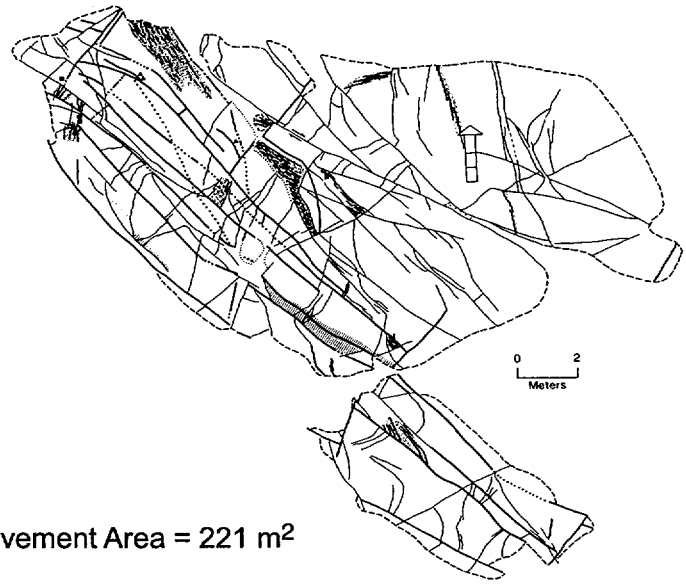

Pavement Area = 221 m^2

Fig. 3
Dunne et al.

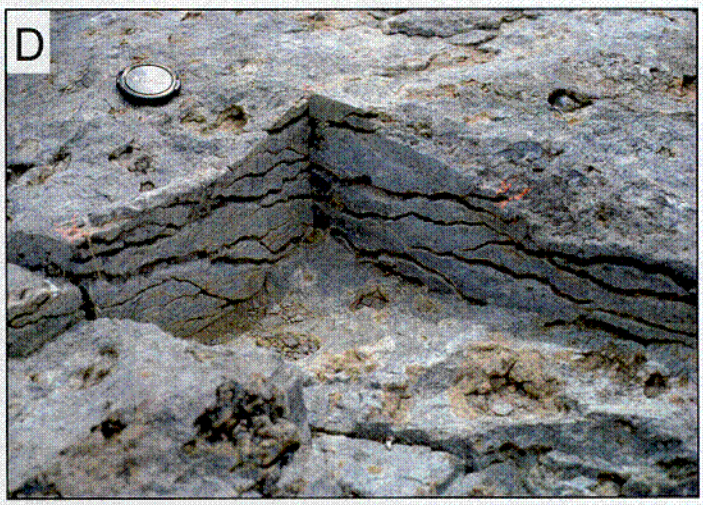

Fig. 4 A, B, C, D
Dunne et al.

C03

(E)

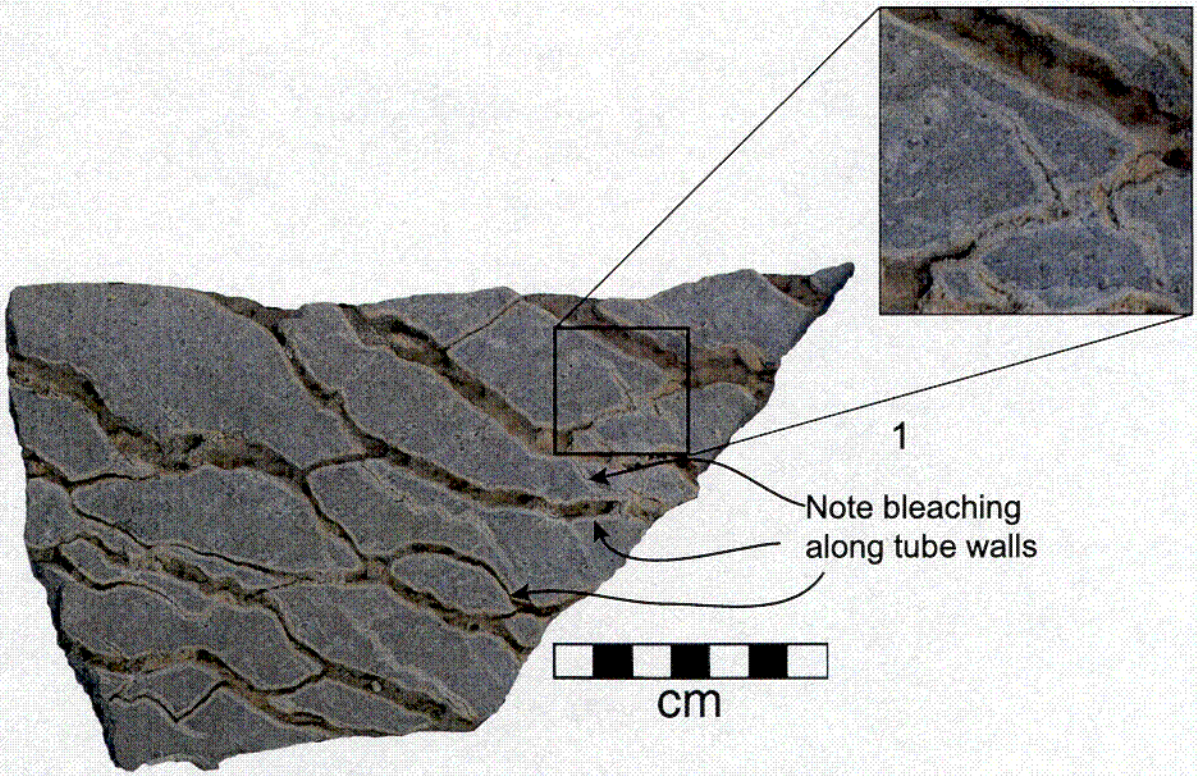

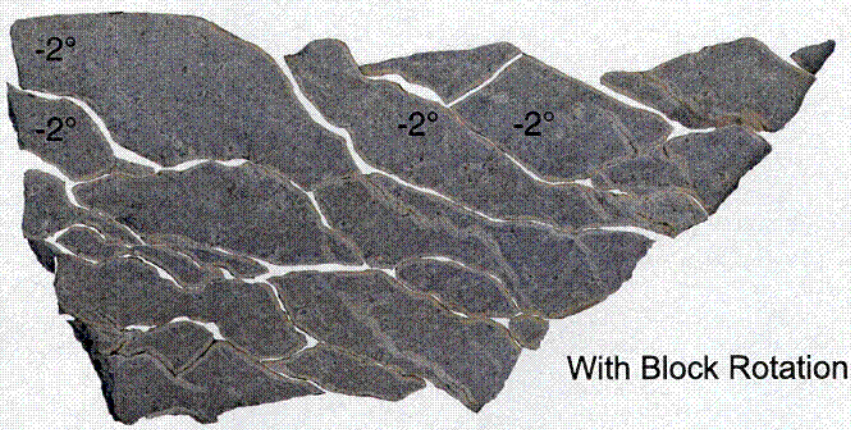

Fig. 4 E
Dunne et al.

C04

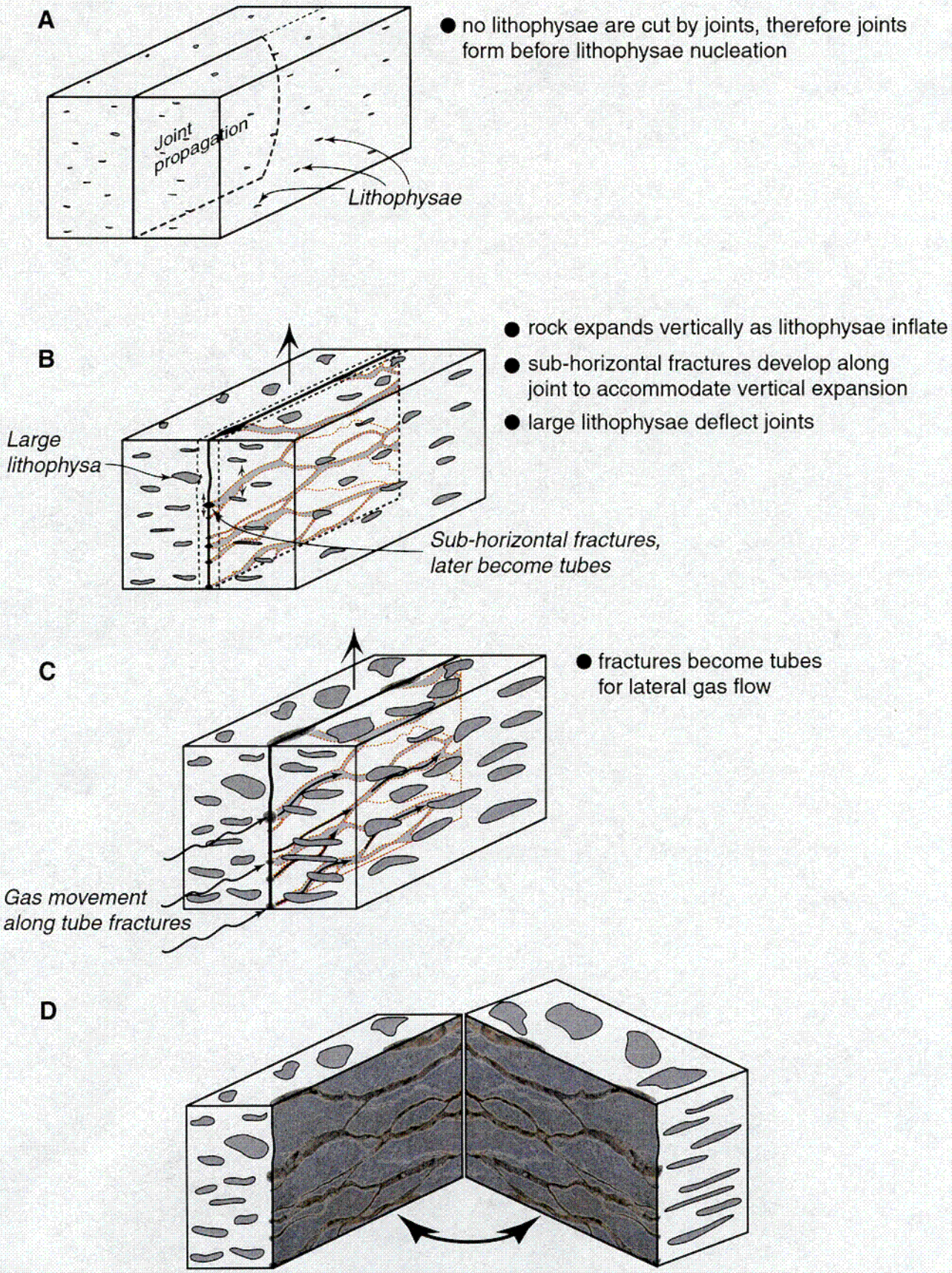

Fig. 5
Dunne et al.

C05

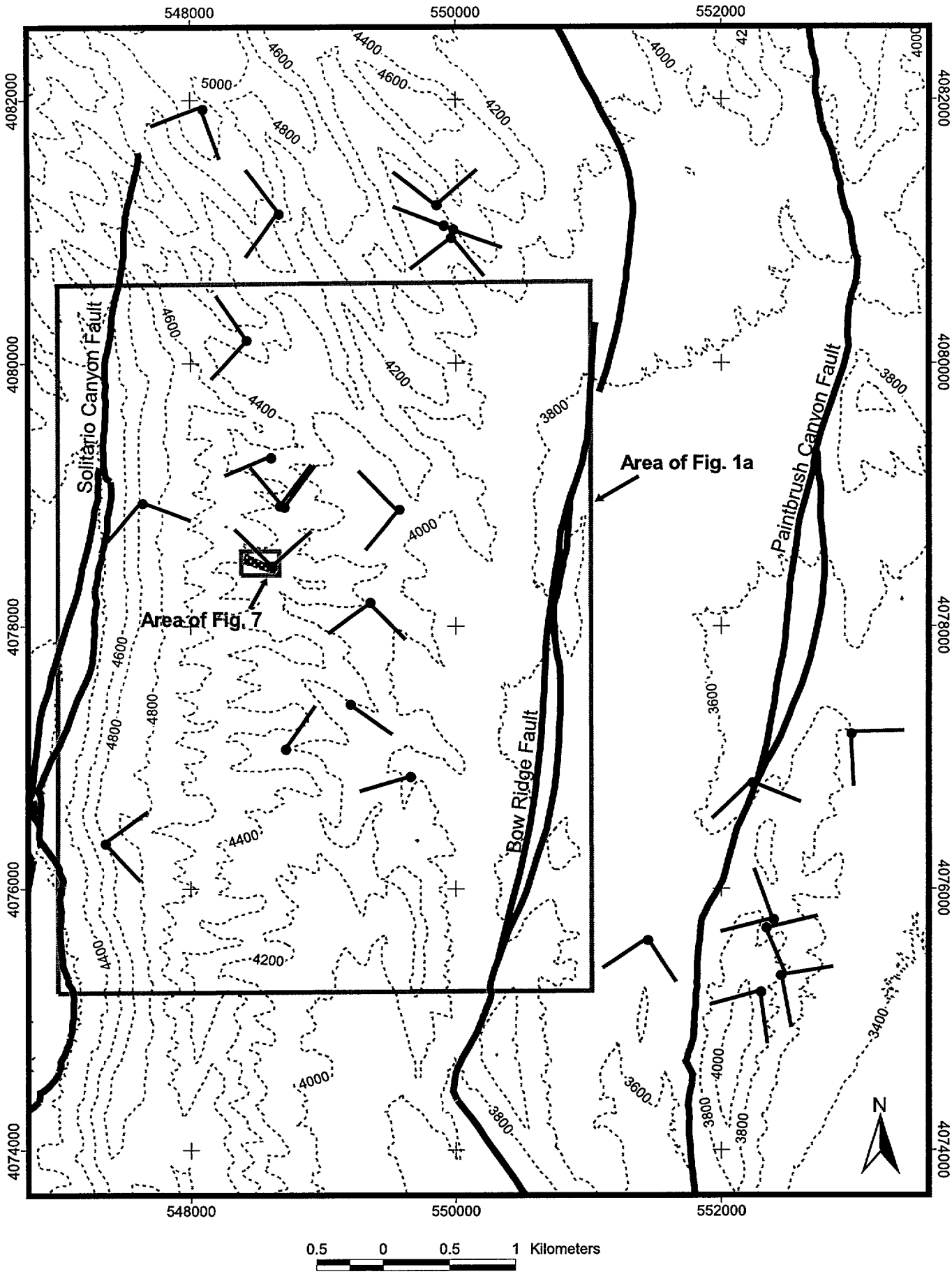

Fig. 6
Dunne et al.

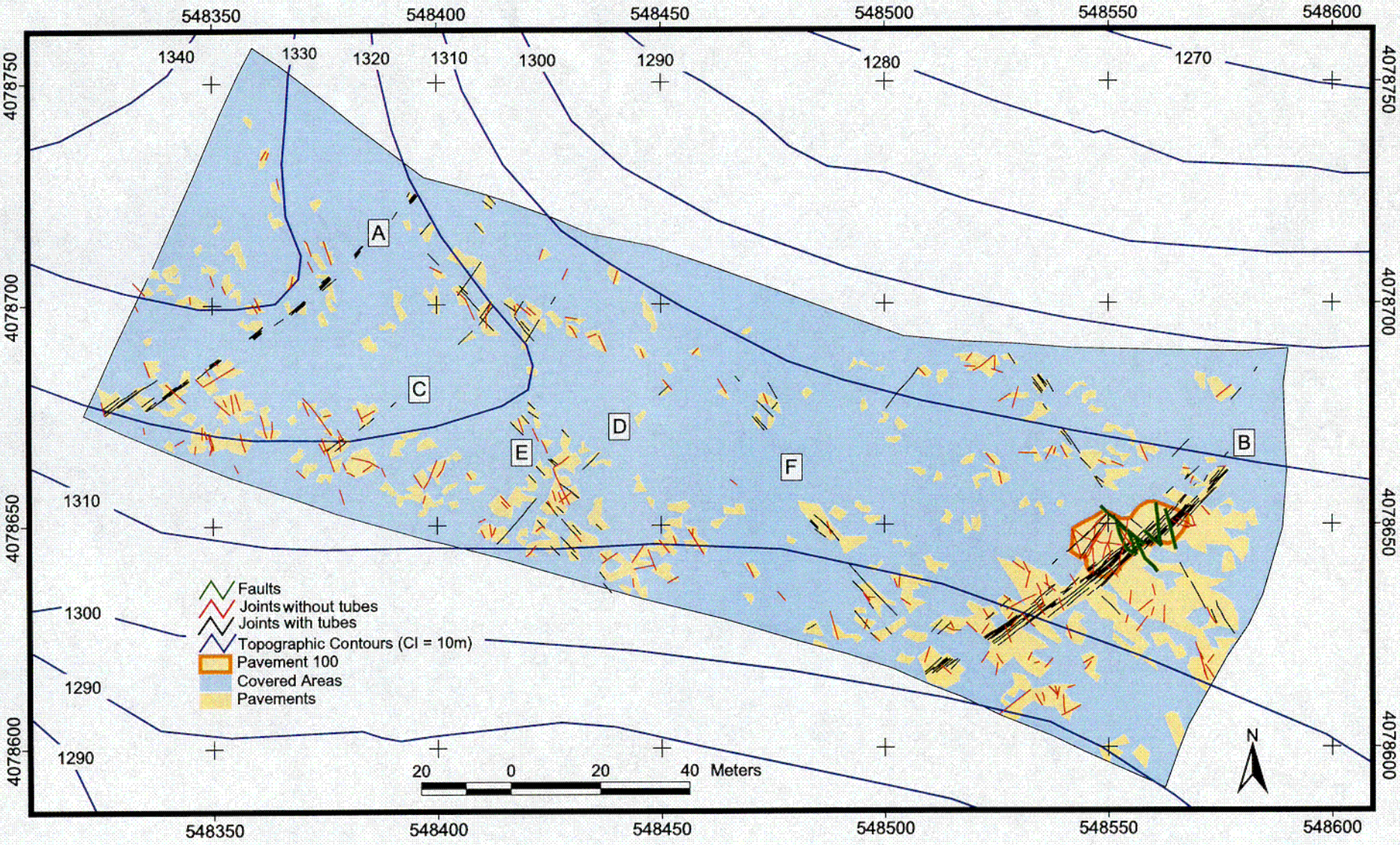

Fig. 7
Dunne et al.

COG

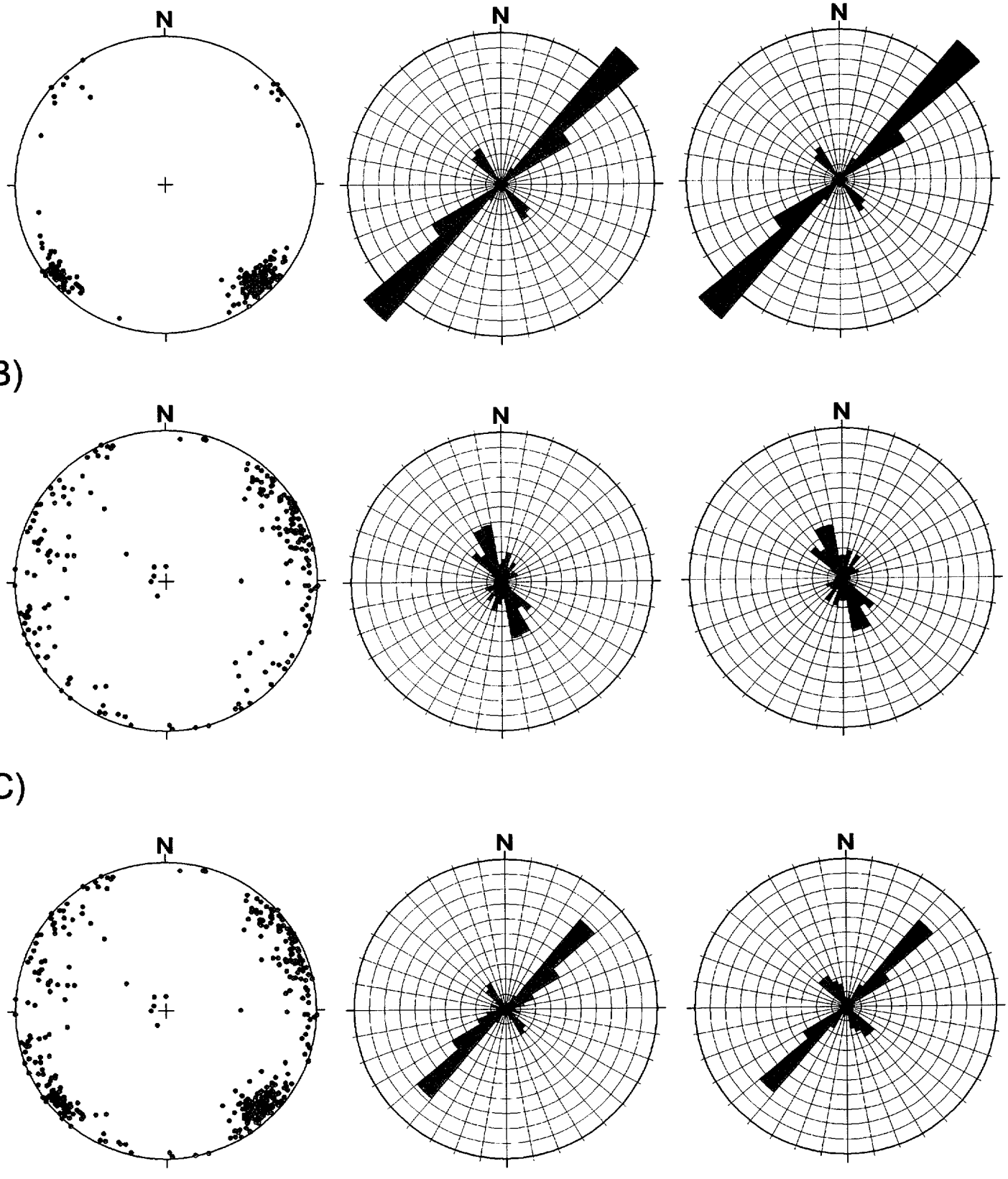

Fig. 8
Dunne et al.

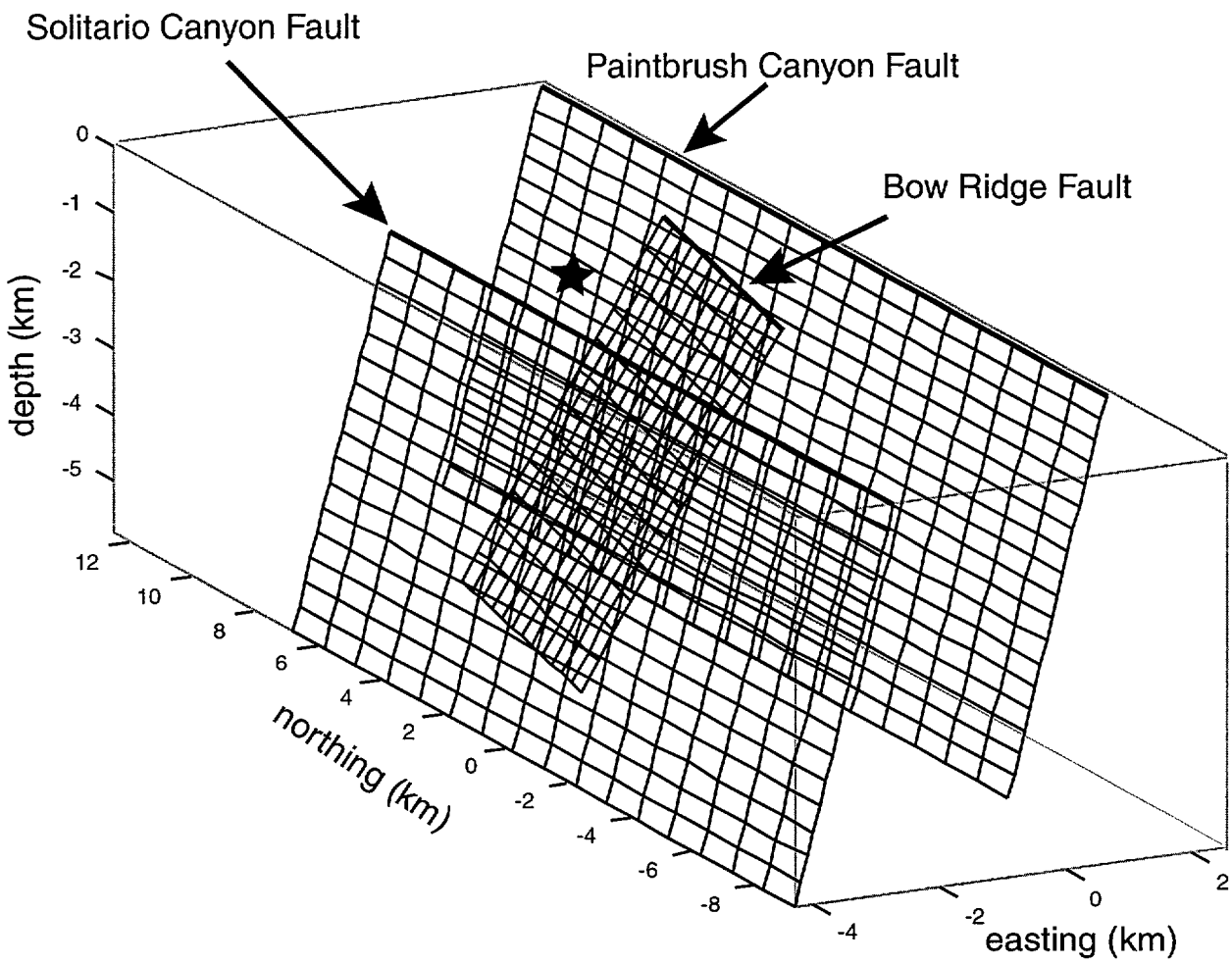

Fig 9
Dunne et al.

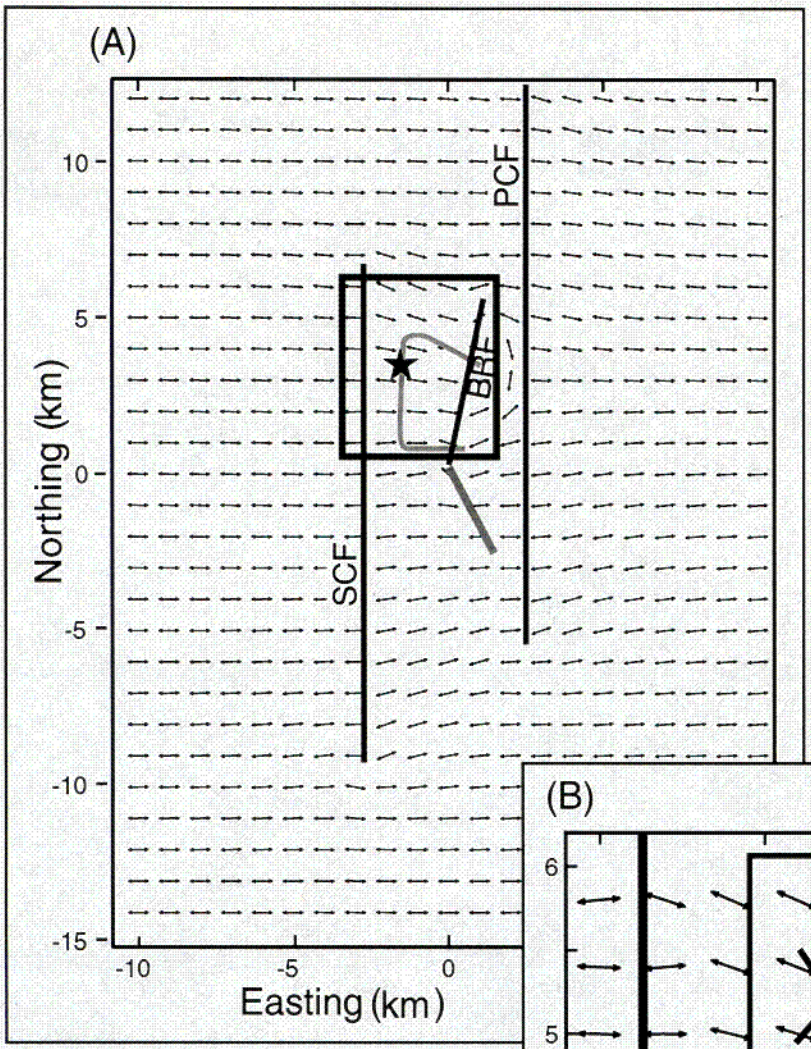

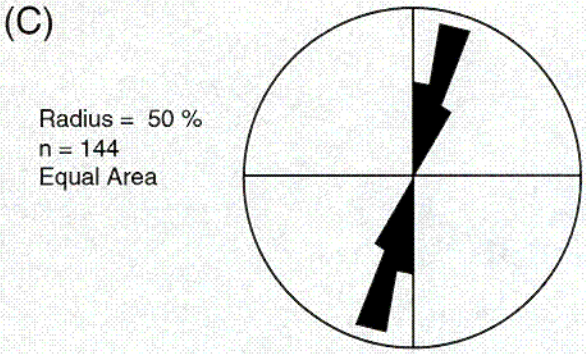

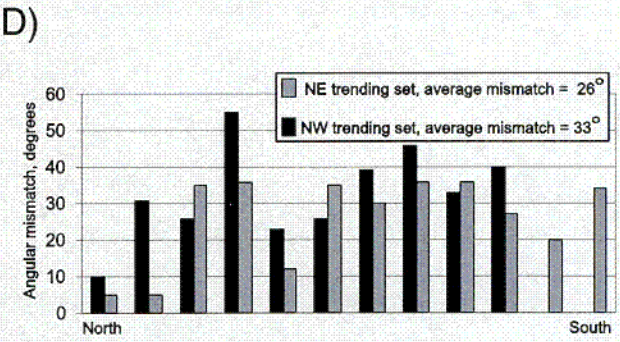

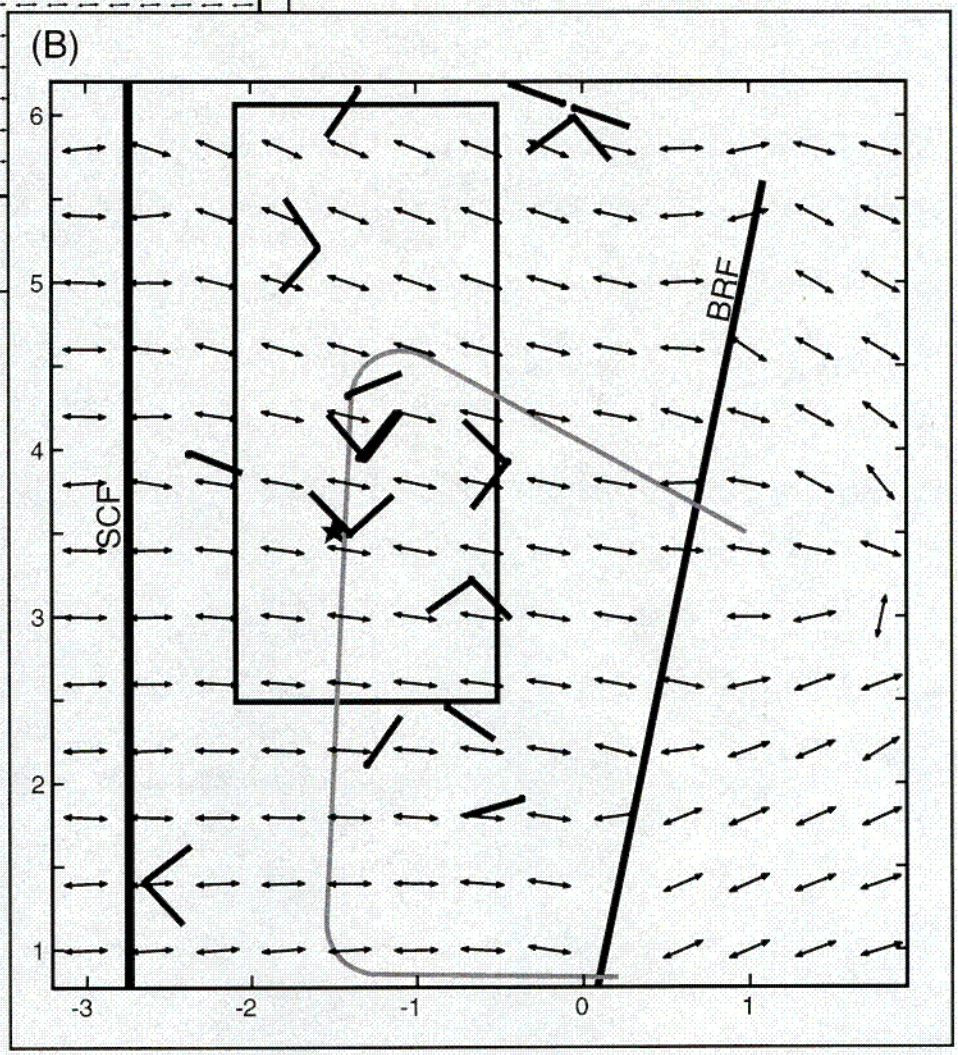

Fig. 10
Dunne et al.

C07

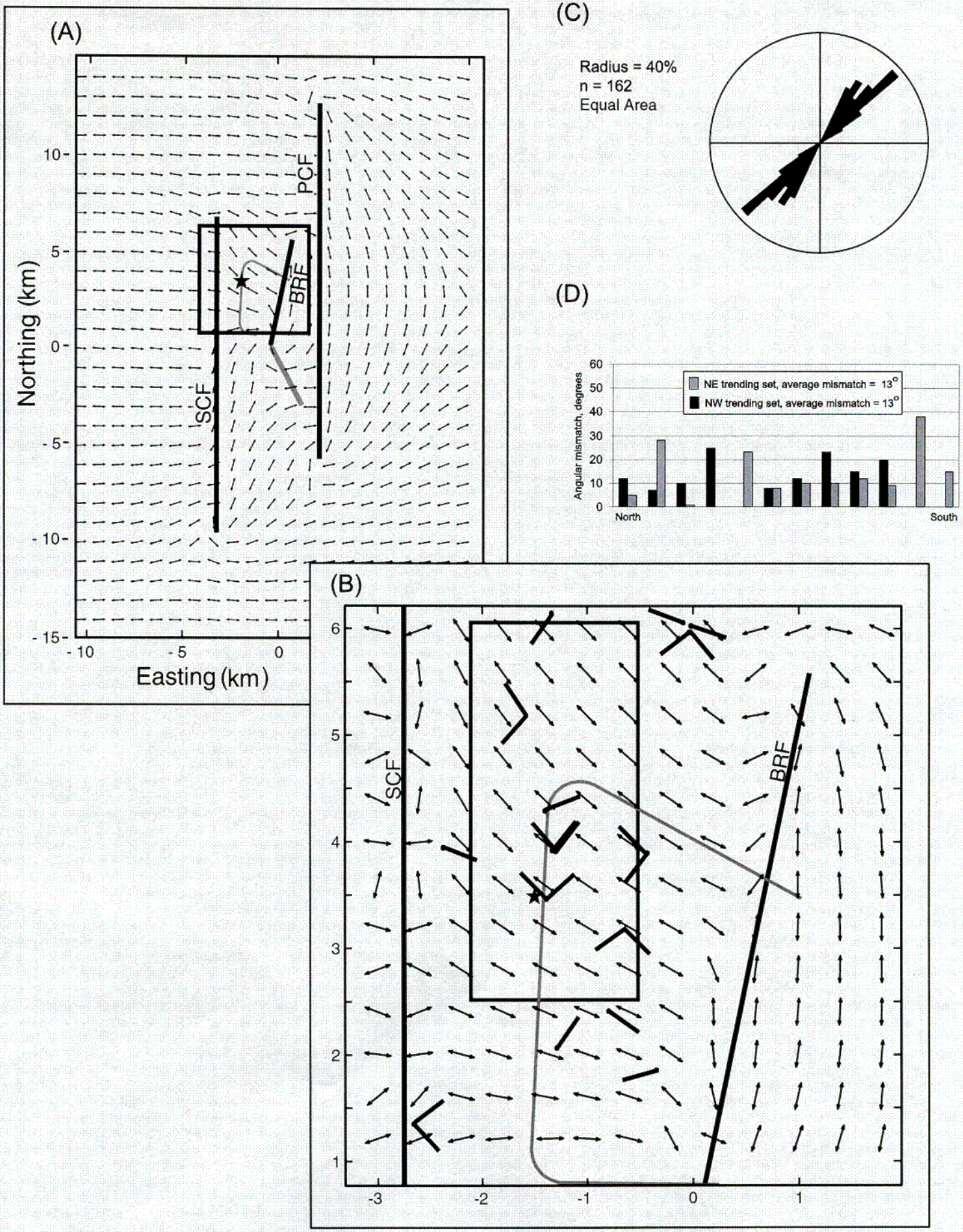

Fig. 11
Dunne et al.

C08